or anti–mouse-IgG (H + L)-conjugated antibodies (Molecular Probe Inc., Eugene, OR) as second antibodies.

For the evaluation of fibrosis, picro-sirius red staining was performed using 0.1% picro-sirius red solution as previously described.[14]

Quantitative Analysis of Liver Fibrosis. We quantified the liver fibrosis area with picro-sirius red staining using an Olympus Provis microscope equipped with a CCD camera (Tokyo, Japan), as described previously.[15] Briefly, the red area, considered the fibrotic area, was assessed by computer-assisted image analysis with MetaMorph software (Universal Imaging Corporation, Downingtown, PA) at a magnification of ×40. The mean value of 6 randomly selected areas per sample was used as the expressed percent area of fibrosis.

Microarray Analysis. Microarray analysis was performed as described previously.[16]

Briefly, total RNA of liver was isolated using the Atlas Pure Total RNA labeling system (Clontech Laboratories, Inc.) from mice 1 week after BMC transplantation (n = 3) or from mice treated with CCl_4 for 5 weeks (n = 3) according to the manufacturer's recommendations. Differential hybridization analysis was done using an Atlas Mouse complementary DNA expression array (BD Bioscience Clontech, Tokyo, Japan). Complementary DNA probe preparation and hybridization were done according to the manufacturer's recommendations. The array results were scanned with a Strom 840 PhosphoImager (Molecular Dynamics, Sunnyvale, CA) and analyzed with Atlas Image software (BD Bioscience Clontech). The results show the mean values of 3 mice in each group.

Hydroxyproline Content. Hydroxyproline content was determined by a modification of Kivirikko's method, as previously reported.[17] Briefly, liver specimens were weighed, and 20 mg of the freeze-dried sample was hydrolyzed in 6 mol/L HCl at 110°C in an autoclave at a pressure of 1.2 kg force/cm^2 for 24 hours. After centrifugation at 2,000 rpm at a temperature of 4°C for 5 minutes, 2 mL of supernatant was mixed with 50 mL of 1% phenolphthalein and 8 N KOH to obtain a total volume of 5 mL of liquid at pH of 7 to 8. Absorbance was measured at 560 nm. The hydroxyproline content of the liver was expressed as micrograms per gram of wet weight.

In Situ *Hybridization.* *In situ* hybridization was performed essentially as described previously.[18] Briefly, digoxigenin (DIG)-11-UTP–labeled single-stranded RNA probes were prepared with DIG RNA labeling mix and the corresponding T3 or T7 RNA polymerase (Boehringer Mannheim Japan, Tokyo, Japan) according to the manufacturer's instructions. The mouse MMP-9 probe was a 150–base pair fragment from the 3′ untranslated region cloned in the pBluescript (Stratagene, Tokyo, Japan) vector. *In situ* hybridization was performed on tissue sections placed on Superfrost Plus slides postfixed in 4% paraformaldehyde in PBS, rinsed in PBS containing 0.1% active diethyl pyrocarbonate, and prehybridized for 2 hours at 58°C in 50% formamide, 5 × SSC (standard saline citrate), and 40 μg of salmon-sperm DNA per milliliter. Hybridization was carried out at 58°C for 16 hours in a humid chamber with 400 ng of DIG-labeled probe per milliliter diluted in the same solution used for prehybridization. After hybridization, the sections were successively washed in 2 × SSC at room temperature for 30 minutes, 2 × SSC for 1 hour at 65°C, and 0.1 × SSC at 65°C for 1 hour. For the reaction of anti-DIG antibodies, slides were preincubated in buffer A (100 mmol/L Tris, 150 mmol/L NaCl [pH 7.5]), and then with an alkaline phosphatase-coupled anti-DIG antibody (Boehringer Mannheim Japan) diluted 1:5,000 in buffer A containing 0.5% Boehringer blocking reagent for 2 hours at room temperature. The slides were washed in buffer A and then preincubated in buffer C (100 mmol/L Tris, 50 mmol/L $MgCl_2$ [pH 9.5]). Alkaline phosphatase was then revealed as described for 16 to 24 hours at room temperature. The enzymatic reaction was stopped with Tris-ethylenediaminetetraacetic acid (EDTA) for 15 minutes. The slides were rinsed in water for several hours and then dried, cleared in xylene, and mounted directly.

In Situ *Zymography.* *In situ* zymography was performed as described.[19]

The fresh specimens of CCl_4 treated with BMC-transplanted liver tissues (1 week after BMC transplantation) were embedded without fixation in Tissue-Tek optimal cutting temperature compound (Miles, Elkhart, IN). Serial frozen sections were made using a cryostat (MicroM, Walldorf, Germany) and mounted on gelatin films that were coated with 7% gelatin solution (Fuji Photo Film, Tokyo, Japan). The films with sections were incubated for 24 hours at 37°C in a moisture chamber and stained with 1.0% amido black 10B. The gelatin in contact with the proteolytic areas of the sections was digested, and thus zones of enzymic activity were indicated by negative staining. The digested areas in the sections were compared with serial sections stained with hematoxylin-eosin. As a control, liver tissues treated with CCl_4 alone (5 weeks) were used, and the frozen sections were treated in a manner similar to that already described.

Statistical Analysis. Results are presented as the mean ± SD. Differences between groups were analyzed by 1-way ANOVA.

The survival rate was examined using the Breslow-Gehan-Wilcoxon test.

Ethical Considerations. This experiment was reviewed by the Committee of Animal Experiment Ethics at

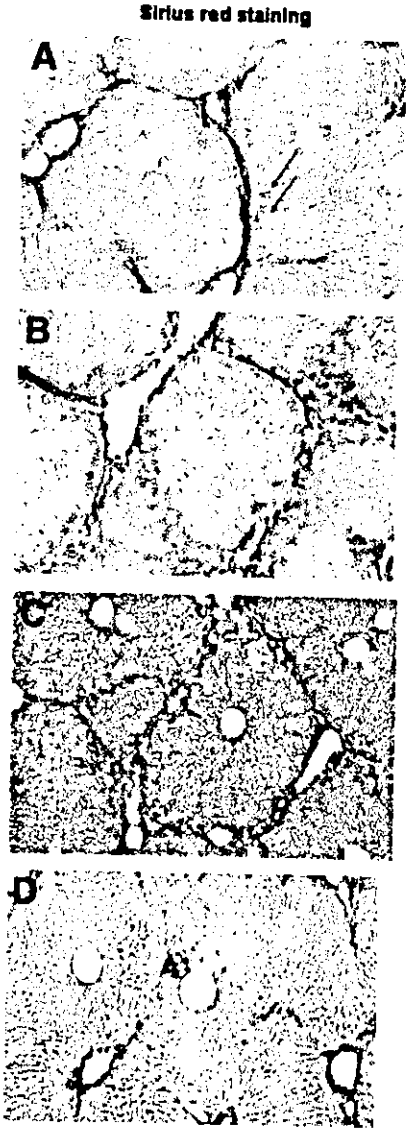

Fig. 1. Photomicrographs of liver sections stained with sirius red from mice after BMC transplantation with continuous CCl_4 treatment. Six-week-old C57BL6 mice were treated with CCl_4 twice a week for 4 weeks. Then, 1×10^5 GFP-positive BMCs were injected through the tail vein. Mice continued to be treated with CCl_4. After (A) 1, (B) 2, (C) 3, and (D) 4 weeks, mice were killed to assess the extent of liver fibrosis. (Original magnification, ×100.)

the Yamaguchi University School of Medicine and was carried out under the guidelines for animal experiments at Yamaguchi University School of Medicine (no. 105).

Results

Five weeks after CCl_4 injection, liver fibrosis was already seen (Supplementary Fig. 1A). One week after BMC transplantation (5 weeks after CCl_4 injection), BMCs were seen along with the fibers recognized by light red staining (black arrows), different from hepatocytes (Fig. 1A) with sirius red staining. More BMCs were seen after 2 weeks (Figs. 1B and 2A,C) and 3 weeks (Figs. 1C and 2B,D), and large spheroid-shaped cells (blue arrows) and small cells (green arrows) (Fig. 2B) were found in the area presumably occupied by fibers (Fig. 2D), shown by sirius red and GFP staining.

Surprisingly, 4 weeks later, the BMC-transplanted liver clearly showed reduction of liver fibrosis (Fig. 1D) compared with the liver treated with CCl_4 alone at 8 weeks (Supplementary Fig. 1D), although CCl_4 was injected throughout the experimental period. Quantitative image analysis of liver fibrosis indicated that the percent area of liver fibrosis at 1 week after BMC transplantation was 5.36% ± 0.90%, but at 4 weeks after transplantation it was significantly decreased to 4.16% ± 0.53% ($P < .001$, n = 8 each; Fig. 3).

Treatment with CCl_4 alone for 8 weeks showed an increased hydroxyproline content of 630 ± 93 μg/wet g liver (Table 1). BMC transplantation significantly reduced this to 392 ± 59 μg/wet g liver 4 weeks later ($P < .01$, n = 8 each). This hydroxyproline content was significantly reduced even compared with that of 1 week after BMC transplantation (494 ± 74 μg/wet g liver, $P < .05$).

The mouse fetal liver at E11.5 functions as a definitive hematopoietic organ, and Liv8-positive cells of the fetal liver at E11.5 include c-kit–positive immature hematopoietic cells and CD45-positive lymphoid cells. These results indicate that almost all Liv8-positive cells are of hematopoietic origin (Supplementary Fig. 2).

In addition, all c-kit–positive mouse adult BMCs belong to the Liv8-positive fraction, and Liv8-positive BMCs include almost all of the CD45- and Thy-1–positive BMCs, in addition to B220, a marker of B lymphocytes (Fig. 4).

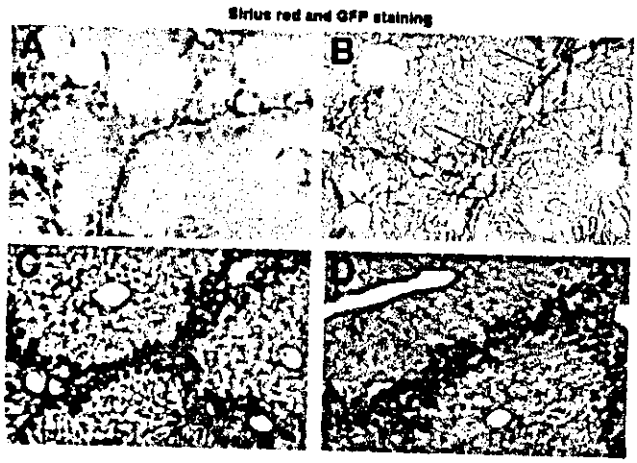

Fig. 2. Photomicrographs of liver sections stained with sirius red or sirius red and GFP from a mouse (A, C) 2 weeks and (B, D) 3 weeks after BMC transplantation. (Original magnification, [A] ×200; [B] ×200; [C] ×200; [D] ×200.)

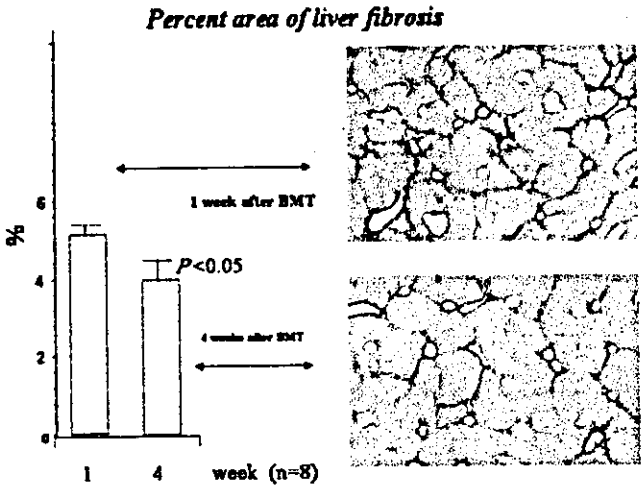

Fig. 3. Quantitatitve analysis of liver fibrosis after bone marrow cell transplantation (BMT). Percent area of liver fibrosis was calculated using sirius red staining as described in Materials and Methods. Results are expressed as mean ± SD of 8 samples. (Original magnification, ×40.)

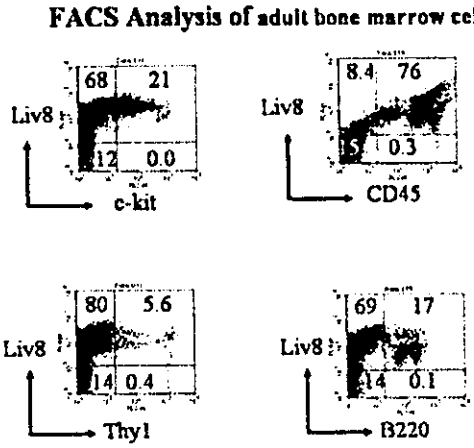

Fig. 4. Expression of Liv8, c-kit, CD45, Thy 1, and B220 in adult BMCs.

These results strongly suggest that Liv8-positive cells include both immature and mature hematopoietic cells.

Liv8-negative BMCs significantly reduced liver fibrosis compared with that of the liver treated with CCl4 alone for 8 weeks, although Liv8-positive BMCs had no effect on liver fibrosis (Table 2).

Microarray analysis of the liver 1 week after BMC transplantation indicated increased expression of MMP-2, MMP-9 and MMP-14 with decreased expression of tissue inhibitor of metalloproteinase-3 (TIMP-3) compared with that of the liver treated with CCl_4 alone for 5 weeks (Table 3). Because the expression of MMP-9 was marked, we investigated it in this model.

Immunohistochemistry of MMP-9 showed localization of these cells similar to that of transplanted BMCs (Fig. 5A). However, the liver treated with CCl_4 alone showed only a few MMP-9–positive nonparenchymal cells (black arrows, Fig. 5B).

The expression of MMP-9 with *in situ* hybridization coincided with the immunohistochemical staining of MMP-9 (Fig. 5C).

Table 1. Hydroxyproline Content

Treatment (No. of Mice)	Hydroxyproline (μg/g Liver)
CCl_4, 5 wk (8)	464 ± 93
CCl_4, 8 wk (8)	630 ± 93
CCl_4/BMT, 5 wk (8)	494 ± 74
CCl_4/BMT, 8 wk (8)	392 ± 59*†

NOTE. Mice were treated with CCl_4 for 4 weeks; then, 1 week or 4 weeks after bone marrow cell transplantation (BMT) or saline injection with CCl_4 treatment, they were killed to measure liver hydroxyproline content. Results are typical of 1 of 3 independent experiments.

*$P < .01$ vs. CCl_4 (8 weeks).

†$P < .05$ vs. CCl_4/BMT (5 weeks).

Although double fluorescent-positive cells were not seen in the liver treated with CCl_4 alone (Fig. 6A), double-positive yellow-colored cells (black arrows) were seen in the BMC-transplanted liver (Fig. 6B). With high magnification, double fluorescent immunohistochemistry showed the expression of MMP-9 (red) on the GFP-positive (green) cell surface (Fig. 6C).

A double fluorescent (anti-GFP with green color and anti–α-smooth muscle actin with red color) study indicated that a fine network pattern of stellate cells (red) existed in the liver treated with CCl_4 alone for 5 weeks (Fig. 7A). Conversely, GFP-positive green-colored cells (green arrow) were seen with a reduced fine network pattern (red arrow) in the liver 1 week after BMC transplantation (Fig. 7B). Double fluorescent-positive yellow-colored cells (yellow arrow), presumably stellate cells, were then seen without the fine network pattern (red arrow) in the liver 2 weeks after BMC transplantation (Fig. 7C). The shape of these cells was different from other GFP-positive cells, and the number of the double-positive cells was very small.

Next, we examined the direct activity of MMP-9 using *in situ* zymography. Film *in situ* zymographic analysis revealed strong gelatinolytic activity in the periportal area

Table 2. Hydroxyproline Content

Treatment (No. of mice)	Hydroxyproline (μg/g Liver)
CCl_4 (8)	687 ± 102
CCl_4/Liv8-positive (8)	638 ± 94
CCl_4/Liv8-negative (8)	415 ± 77*

NOTE. Mice were treated with CCl_4 for 4 weeks followed by transplantation with Liv8-positive or Liv8-negative BMCs or saline. After 4 weeks of CCl_4 treatment (total 8 weeks), mice were killed to measure liver hydroxyproline content. Results are typical of 1 of 3 independent experiments.

*$P < .01$ vs. CCl_4.

Table 3. Microarray Analysis

	CCl_4 + BMC vs. CCl_4 Alone	
	Increased	Decreased
MMP-2	1.7	
MMP-9	3.9	
MMP-14	2.1	
TIMP-3		0.67

NOTE. Mice were treated with CCl_4 for 4 weeks and were killed 1 week after BMC transplantation. Microarray analysis was performed using 3 livers from each group. The expression ratios (CCl_4 + BMC vs. CCl_4 alone) larger than 1.5 are shown. Values indicated are the difference between the mean values of 3 mice. Results are typical of 1 of 2 independent experiments.

coinciding with the location of MMP-9–positive BMCs compared with the liver treated with CCl_4 alone (Fig. 8).

This gelatinolytic activity was completely blocked by the addition of 1,10-phenanthroline, an MMP inhibitor (data not shown).

Finally, the mice that underwent BMC transplantation with continuous CCl_4 injection showed a gradually increased serum albumin level (Supplementary Fig. 3) resulting in a significantly improved survival rate after BMC transplantation compared with mice treated with CCl_4 alone (Supplementary Fig. 4).

Discussion

In this report, transplanted BMCs can degrade collagen fibers and clearly reduce liver fibrosis with strong expression of MMPs, especially MMP-9, as indicated by both *in situ* zymography and the double staining of GFP and MMP-9 using fluorescent microscopy. The reason for the strong expression of MMP-9 is still unknown.

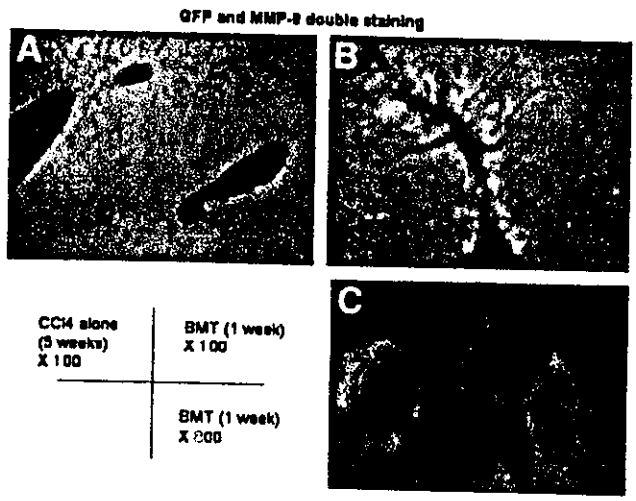

Fig. 6. Double fluorescent immunohistochemistry of a mouse liver after (A) 5-week treatment with CCl_4 alone and (B, C) 1 week after BMC transplantation (BMT) with CCl_4 treatment for 5 weeks. (Original magnification, [A and B] ×100; [C] ×800.)

However, Heissing et al.[20,21] recently reported that MMP-9 induced in BMCs released soluble Kit-ligand, which might be related to the transfer of stem cells in BMCs to the proliferative niche. Therefore, MMP-9 in our model could play an important role in the degradation of extracellular matrix and also by releasing some factors, *e.g.*, soluble Kit-ligand, related to the differentiation and proliferation of transplanted BMCs in liver inflammation induced by continuous injection of CCl_4. It has also been shown that MMP-9 plays an important role in the migration of mast progenitor cells to inflammatory

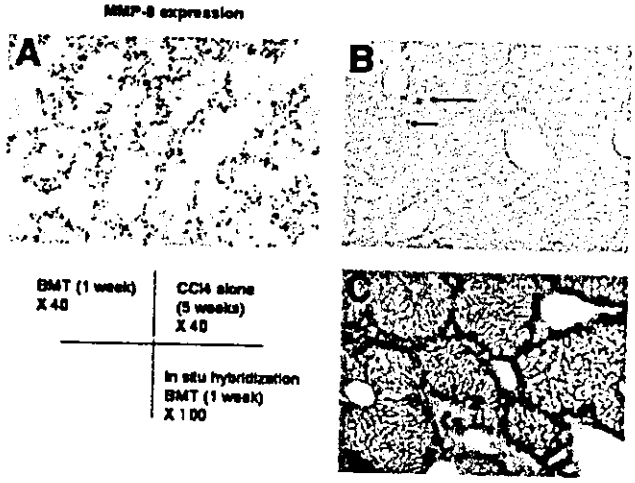

Fig. 5. Photomicrograph of a liver section stained with anti-MMP-9 antibody (A) from a mouse 1 week after BMC transplantation (BMT) and (B) from a mouse treated with CCl_4 alone for 5 weeks. (Original magnification, ×40.) (C) *In situ* hybridization of a liver section from a mouse 1 week after BMC transplantation. (Original magnification, ×100.)

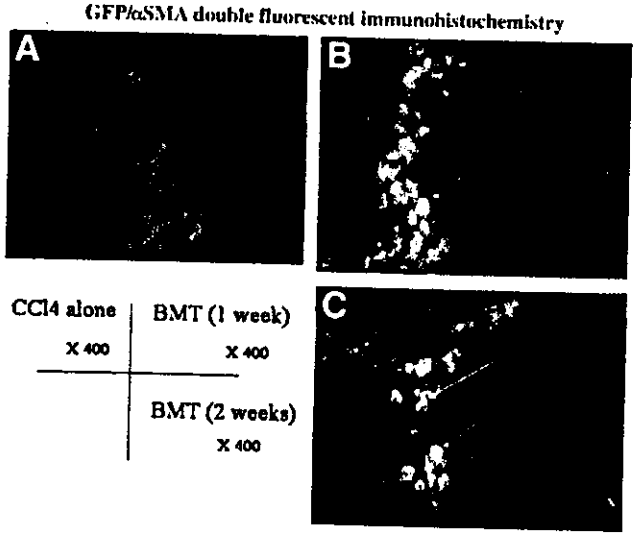

Fig. 7. Double fluorescent immunohistochemistry for α-smooth muscle actin (αSMA) and GFP of a mouse liver (A) treated with CCl_4 alone for 5 weeks and (B) 1 week, or (C) 2 weeks after BMC transplantation (BMT) with CCl_4 treatment. (Original magnification, ×400.)

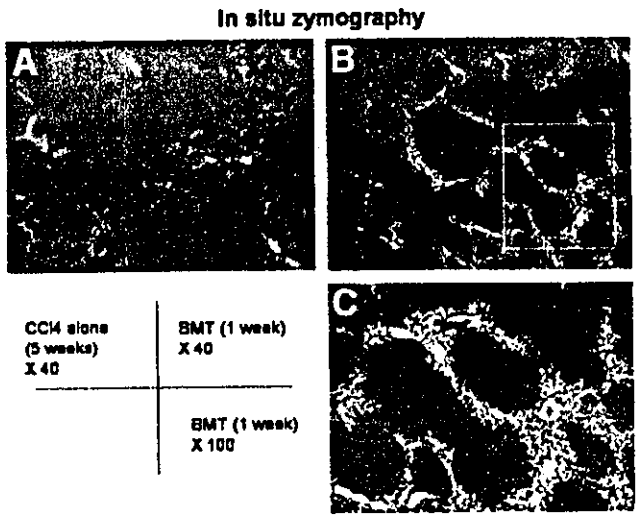

Fig. 8. *In situ* zymography of a mouse liver after (A) 5-week treatment with CCl_4 alone and (B, C) 1 week after BMC transplantation (BMT) with CCl_4 treatment for 5 weeks. (Original magnification, [A] ×40; [B] ×40, [C] ×100.)

tissue.[22,23] Therefore, the increased expression of MMP-9 in this study was somehow related to the migration of BMCs to the inflammatory liver.

Film *in situ* zymography clearly showed that these MMP-9–positive cells possessed high gelatinolytic activity compared with the liver treated with CCl_4 alone. Thus, the BMCs that migrated acted in the degradation of liver fibrosis (fibrolysis).

According to our present data, increased expression of MMP-14 (MT1-MMP [membrane-type 1 matrix metalloproteinase]) will contribute to degrading interstitial collagens[24] to gelatin that MMP-9 can degrade, resulting in the regression of fibrosis (fibrolysis).

Recently, Kollet et al.[25] reported that the expression of MMP-9 was increased with the migration of human $CD34^+$ progenitor cells in CCl_4-treated NOD/SCID mice and that an inhibitor of MMP-9 reduced this migration. Thus, proteolytic activity seems to be necessary for the cell migration in addition to matrix degradation activity.

It seems to be very important how many cells can migrate into the damaged liver to degrade fibers, but a recent paper[26] reported little evidence of bone marrow-derived hepatocytes in the CCl_4-treated liver. However, the dose of CCl_4 was only 4% (0.08 mL/kg) of our dose (0.5 mL/kg), and the number of mice used was too small (1 or 2). The reason they did not see the BMCs that migrated is most likely due to the cessation of CCl_4 injection after BMC transplantation. Even in our experimental model,[11] the cessation of CCl_4 after BMC transplantation dramatically reduced the number of BMCs migrating into the damaged liver (I.S., unpublished data, 2003). Thus, the extent of continuing liver damage may limit BMC migration to the liver with matrix degradation activity.

Transplanted BMCs differentiated into albumin-producing hepatocytes with an increased serum albumin level, and the degradation of the extracellular matrix may presumably lead to improved liver function resulting in better survival of mice with BMCtransplantation compared to that of treated with CCl_4 alone, although only 1 transplantation of BMCs was performed.

As shown by double fluorescence, our data may also indicate that transplanted BMCs seem to become stellate cells, in agreement with a recent report,[27] although the number was very small in our experimental model. This result seems to be contradictory to our result of resolution of liver fibrosis by BMC transplantation because transdifferentiated stellate cells may produce collagens. Our preliminary results indicated reduced messenger RNA expression of type I procollagen, transforming growth factor-β1 (TGF-β1) and no change of hepatocyte growth factor messenger RNA expression in the liver 1 week after BMC transplantation compared with the liver treated with CCl_4 alone (I. Sakaida, unpublished data, 2003). As shown in Fig. 7, migrated BMCs seemed to reduce the fine network pattern of activated stellate cells. Thus, transplanted BMCs may affect activated stellate cells by reducing their number—*e.g.*, by leading them to apoptosis. However, further examinations are necessary to determine the exact relationship between BMCs and resident stellate cells.

Our recent data[12] indicated that the subpopulation of BMCs, nonhematopoietic cells in bone marrow, separated using an anti-Liv8 antibody, will transdifferentiate into hepatocytes in the liver damaged by CCl_4 induction. The present study clearly indicates that this subpopulation of BMCs is also responsible for the resolution of liver fibrosis (fibrolysis) induced by CCl_4 treatment.

In conclusion, the present study introduces a new concept for the treatment of liver fibrosis.

References

1. Petersen BE, Bowen WC, Patrene KD, Mars WM, Sullivan AK, Murase N, et al. Bone marrow as a potential source of hepatic oval cells. Science 1999;284:1168–1170.
2. Theise ND, Nimmakayalu M, Gardner R, Illei PB, Morgan G, Teperman L, et al. Liver from bone marrow in humans. HEPATOLOGY 2000;32:11–16.
3. Alison MR, Poulsom R, Jeffery R, Dhillon AP, Quaglia A, Jacob J, et al. Hepatocytes from nonhepatic adult stem cells. Nature 2000;406:257.
4. Krause DS, Theise ND, Collector MI, Henegariu O, Hwang S, Gardner R, et al. Multi-organ, multi-lineage engraftment by a single bone marrow-derived stem cell. Cell 2001;105:369–377.
5. Lagasse E, Connors H, Al-Dhalimy M, Reitsma M, Dohse M, Osborne L, et al. Purified hematopoietic stem cells can differentiate into hepatocytes in vivo. Nat Med 2000;6:1229–1234.

6. Orlic D, Kajstura J, Chimenti S, Jakoniuk I, Anderson SM, Li B, et al. Bone marrow cells regenerate infarcted myocardium. Nature 2001;410: 701–705.
7. Korbling M, Katz RL, Khanna A, Ruifrok AC, Rondon G, Albitar M, et al. Hepatocytes and epithelial cells of donor origin in recipients of peripheral-blood stem cells. N Engl J Med 2002;346:738–746.
8. Okamoto R, Yajima T, Yamazaki M, Kanai T, Mukai M, Okamoto S, et al. Damaged epithelia regenerated by bone marrow-derived cells in the human gastrointestinal tract. Nat Med 2002;8:1011–1017.
9. Wagers AJ, Sherwood RI, Christensen JL, Weissman IL. Little evidence for developmental plasticity of adult hematopoietic stem cells. Science 2002; 297:2256–2259.
10. Okabe M, Ikawa M, Kominami K, Nakanishi T, Nishimune Y. "Green mice" as a source of ubiquitous green cells. FEBS Lett 1997;407:313–319.
11. Terai S, Sakaida I, Yamamoto N, Omori K, Watanabe T, Ohata S, et al. An in vivo model for monitoring trans-differentiation of bone marrow cells into functional hepatocytes. J Biochem (Tokyo). 2003;134:551–558.
12. Yamamoto N, Terai S, Ohata S, Watanabe T, Omori K, Shinoda K, et al. A subpopulation of bone marrow cells depleted by a novel antibody, anti-Liv8, is useful for cell therapy to repair damaged liver. Biochem Biophys Res Commun 2004;313:1110–1118.
13. Watanabe T, Nakagawa K, Ohata S, Kitagawa D, Nishitai G, Seo J, et al. SEK1/MKK4-mediated SAPK/JNK signaling participates in embryonic hepatoblast proliferation via a pathway different from NF-kappaB-induced anti-apoptosis. Dev Biol 2002;250:332–347.
14. Sakaida I, Uchida K, Matsumura Y, Okita K. Interferon gamma treatment prevents procollagen gene expression without affecting transforming growth factor-beta1 expression in pig serum-induced rat liver fibrosis in vivo. J Hepatol 1998;28:471–479.
15. Sakaida I, Nagatomi A, Hironaka K, Uchida K, Okita K. Quantitative analysis of liver fibrosis and stellate cell changes in patients with chronic hepatitis C after interferon therapy. Am J Gastroenterol 1999;94:489–496.
16. Sakaida I, Tsuchiya M, Kawaguchi K, Kimura T, Terai S, Okita K. Herbal medicine Inchin-ko-to (TJ-135) prevents liver fibrosis and enzyme-altered lesions in rat liver cirrhosis induced by a choline-deficient L-amino acid-defined diet. J Hepatol 2003;38:762–769.
17. Sakaida I, Hironaka K, Uchida K, Suzuki C, Kayano K, Okita K. Fibrosis accelerates the development of enzyme-altered lesions in the rat liver. HEPATOLOGY 1998;28:1247–1252.
18. Jimenez MJ, Balbin M, Lopez JM, Alvarez J, Komori T, Lopez-Otin C. Collagenase 3 is a target of Cbfa1, a transcription factor of the runt gene family involved in bone formation. Mol Cell Biol 1999;19:4431–4442.
19. Nakada M, Nakamura H, Ikeda E, Fujimoto N, Yamashita J, Sato H, et al. Expression and tissue localization of membrane-type 1, 2, and 3 matrix metalloproteinases in human astrocytic tumors. Am J Pathol 1999;154: 417–428.
20. Heissig B, Hattori K, Dias S, Friedrich M, Ferris B, Hackett NR, et al. Recruitment of stem and progenitor cells from the bone marrow niche requires MMP-9 mediated release of kit-ligand. Cell 2002;109:625–637.
21. Hattori K, Heissig B, Wu Y, Dias S, Tejada R, Ferris B, et al. Placental growth factor reconstitutes hematopoiesis by recruiting VEGFR1(+) stem cells from bone-marrow microenvironment. Nat Med 2003;8:841–849.
22. Tanaka A, Arai K, Kitamura Y, Matsuda H. Matrix metalloproteinase-9 production, a newly identified function of mast cell progenitors, is down-regulated by c-kit receptor activation. Blood 1999;94:2390–2395.
23. Baram D, Vaday GG, Salamon P, Drucker I, Hershkoviz R, Mekori YA. Human mast cells release metalloproteinase-9 on contact with activated T cells: juxtacrine regulation by TNF-alpha. J Immunol 2001;167:4008–4016.
24. Ohuchi E, Imai K, Fujii Y, Sato H, Seiki M, Okada Y. Membrane type 1 matrix metalloproteinase digests interstitial collagens and other extracellular matrix macromolecules. J Biol Chem 1997;272:2446–2451.
25. Kollet O, Shivtiel S, Chen YQ, Suriawinta J, Thung SN, Dabeva MD, et al. HGF, SDF-1, and MMP-9 are involved in stress-induced human CD34+ stem cell recruitment to the liver. J Clin Invest 2003;112:160–169.
26. Kanazawa Y, Verma IM. Little evidence of bone marrow-derived hepatocytes in the replacement of injured liver. Proc Natl Acad Sci U S A 2003; 100(Suppl);11850–11853.
27. Forbes SJ, Russo FP, Rey V, Burra P, Rugge M, Wright NA, et al. A significant proportion of myofibroblasts are of bone marrow origin in human liver fibrosis. Gastroenterology 2004;126:955–963.

FEBS Letters 578 (2004) 10–20

FEBS 28981

Molecular signature associated with plasticity of bone marrow cell under persistent liver damage by self-organizing-map-based gene expression ☆

Kaoru Omori[a], Shuji Terai[a,*], Tsuyoshi Ishikawa[a], Kouji Aoyama[a], Isao Sakaida[a], Hiroshi Nishina[b], Koh Shinoda[c], Shunji Uchimura[d], Yoshihiko Hamamoto[d], Kiwamu Okita[a]

[a] *Department of Molecular Science and Applied Medicine (Gastroenterology and Hepatology), Yamaguchi University School of Medicine, Minami Kogushi 1-1-1, Ube, Yamaguchi 755 8505, Japan*

[b] *Department of Physiological Chemistry, Graduate School of Pharmaceutical Science, University of Tokyo, Hongo 7-3-1, Bunkyoku, Tokyo 113 0033, Japan*

[c] *Department of Neuroanatomy and Neuroscience, Yamaguchi University School of Medicine, Minami Kogushi 1-1-1, Ube, Yamaguchi 755 8505, Japan*

[d] *Department of Computer Science and Systems Engineering, Faculty of Engineering, Yamaguchi University, Tokiwadai 2-16-1, Ube, Yamaguchi 755 8505, Japan*

Received 22 April 2004; revised 3 September 2004; accepted 23 September 2004

Available online 2 November 2004

Edited by Gianni Cesareni

Abstract **The mechanism that regulates the plasticity of bone marrow cells (BMCs) into hepatocytes is poorly understood. We developed a green fluorescent protein/carbon tetrachloride model to find that BMC transplantation recovered liver damage. Serum albumin level and liver fibrosis were recovered by BMC transplantation. To understand the mechanism, we used DNA-chip technology to profile the change of transient gene expression before and after BMC transplantation. On the basis of gene expression with self-organizing map using specific equation, genes were classified into 153 clusters. The information is useful to understand the dramatic gene activation during the process of the plasticity of BMC.**

Keywords: Bone marrow cell; Plasticity; Regenerative Medicine; Gene expression; Microarray analysis; Self-organizing map; Liver regeneration

1. Introduction

Recently, several groups have reported the possible plasticity of bone marrow cells (BMC) to differentiate into a variety of non-hematopoietic cell lineages [1,2]. Ever since, the differentiation of BMC into hepatocytes in human was documented following a bone marrow transplantation from a man to a woman [3]. The mechanism of the plasticity of BMC was discussed whether that was occurred with cell fusion, nuclear reprogramming [4–6] or trans-differentiation [7,8]. We think both cell fusion and trans-differentiation might be important to understand the mechanism of BMC plasticity. On the other hand, in cardiovascular medicine, clinical research has been conducted to evaluate the use of BMCs in regenerating the myocardium and vessels, and some positive results have been obtained [9,10]. These findings suggest the usefulness of BMCs as the source of cells in developing the next-generation of treatment for liver regeneration [11]. We first tried to understand how we could use BMC to repair damaged liver. We have developed a model [named as a green fluorescent protein/carbon tetrachloride (GFP/CCl_4)] to evaluate the usefulness of BMC transplantation for damaged liver [12,13]. In this model, 0.5 ml/kg of carbon tetrachloride (CCl_4) is administered twice weekly to induce liver cirrhosis and then GFP-positive BMCs are transplanted through the causal vein [14]. Under continuous liver injury, immunostaining using anti-GFP antibodies [15] showed that GFP-positive BMCs migrated into the marginal area of the hepatic lobule starting from day 1 after BMC transplantation, and with time, while forming a hepatic cord towards the central vein, the distribution of GFP-positive BMCs expands [12,16]. Also, using Liv2, a hepatoblast-specific antibody that we developed [17], it has been shown that BMCs first trans-differentiate into Liv2-positive hepatoblasts and then differentiated into albumin-positive hepatocytes. Furthermore, the level of serum albumin significantly increases with time in recipient mice. Liver fibrosis induced by CCl_4 injection was recovered by BMC transplantation [18]. These findings suggest that this GFP/CCl_4 model can be used

☆ Grant Support: This study was supported by Grants-in-Aid for Scientific Research from the Japan Society for the Promotion of Science (Nos. 13470121, 13770262, 15790348, *16390211* and *16590597*) and for translational research from the Ministry of Health, Labor and Welfare (H-trans-5).

* Corresponding author. Fax: +81-836-222-240.
E-mail address: terais@yamaguchi-u.ac.jp (S. Terai).

Abbreviations: BMC, bone marrow cell; SOM, self-organizing map; CCl_4, carbon tetrachloride; EGFP, enhanced GFP; GFP, green fluorescent protein; RT, reverse transcriptase; HNF4-α, hepatocyte nuclear factor 4 alpha; VEGF, vascular endothelial growth factor; HGF, hepatocyte growth factor; FAH, fumarylacetoacetate hydrolase; TNFR, tumor necrosis factor receptor; FGF, fibroblast growth factor; MMP, matrix metalloproteinase; TIMP, tissue inhibitor of metalloproteinase; NumbL, Numblike; HOX, homeobox; GPI, glucose-6-phosphatase isomerase

0014-5793/$22.00 © 2004 Published by Elsevier B.V. on behalf of the Federation of European Biochemical Societies.
doi:10.1016/j.febslet.2004.09.090

to understand the process of plasticity of BMCs under persistent liver damage condition. It is important to understand what had happened in GFP/CCl_4 model after BMC transplantation in mRNA level. DNA chips are recently developed tools used in genetic analyses [19]. While it is possible to obtain genetic data using DNA chips, the vast amount of information collected makes it difficult to precisely interpret the factors involved in the gene expression. Therefore, in the present study, patterns of global gene expression at different times were compared between mice with BMC transplantation and those without. Self-organizing map (SOM) is a statistical technique that has been recently used in analyzing microarray data and, via this method, it is possible to visualize a vast amount of complicated and multidimensional data [20]. In this analysis, we made a specific equation to extract genes with expressions that altered in relation to BMC transplantation. Here, we present the results obtained from this study.

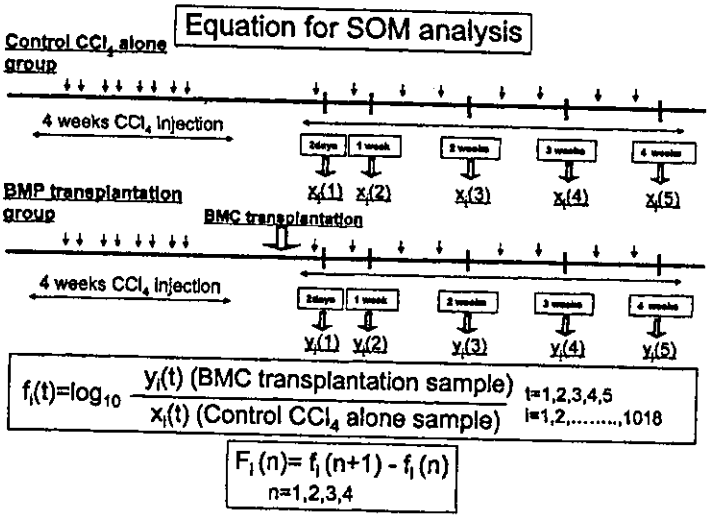

Fig. 1. Defined equation in this analysis. (1) Arrow indicates CCl_4 injection twice a week in GFP/CCl_4 model. We analyzed gene expression in each time point (2 days, 1 week, 2 weeks, 3 weeks, and 4 weeks). $y_i(t)$ showed the gene expression level of the liver after BMC transplantation. $x_i(t)$ showed the gene expression level of the liver CCl_4 alone injection group. We define $f_i(t)$: $f_i(t) = \log_{10} y_i(t)/x_i(t)$. By using this, we succeeded in extracting the change of gene expression by BMC transplantation. We are interested in following the change of the values of $F_i(t) = f_i(t+1) - f_i(t)$ with the increase in t.

Table 1
Lists of primers for selected 13 genes

Cluster	Gene name (Accession No.)	Primer – forward (5′–3′) Primer – reverse (5′–3′)	Target	Tm
86	c-kit (NM02099)	TCCAACGATGTGGGCAAGAG AATGAGCAGCGGCGTGAA	90	55
86	FGP6 (M92415)	CATGGTCTATACCGGCCACA GGCTGCTGACATGAAACCAAAG	88	63
125	MMP2 (NM008610)	CCCTGATGTCCAGCAAGTAGATG ATTCCAGGAGTCTGCGATGAG	148	62
125	MMP9 (NM013599)	ACGACATAGACGGCATCCAGTA TCGGCTGTGGTTCAGTTGTG	90	53
92	TIMP2 (NM011594)	ACACGCTTAGCATCACCCAGA TGTGACCCAGTCCATCCAGAG	137	63
13	HGF (NM010427)	CCCAAACATCCGAGTTGGCTAC TTCCCATTGCCACGATAACA	84	63
1	NumbL (NM010950)	TATGCAGCCTCCGTTTGTG GCGTTGGCTACCATCTGTGAA	102	62
1	HOXD3 (NM010468)	CCATAAATCAGCCGCAAGGA GGATGGGTCGAGGACTTACCTTAG	112	63
152	GPI (NM008155)	TGGACGGCAAAGATGTGATG CGATGTTGATGATGTCCGTGA	129	63
152	VEGF (NM009505)	ATGCGGATCAAACCTCACCA CCGCTCTGAACAAGGCTCAC	129	63
136	TNFR1 (NM011609)	CTGCTCTACGAATCACTCTGCTC ACAGCATACAGAATCGCAAGGTC	113	62
151	HNF4 (NM008261)	CCAAGTACATCCCGGCCTTC CTAGGAGCAGCACGTCCTTAAAC	132	62
151	FGF2 (NM008006)	GGCTGCTGGCTTCTAAGTGTG ACTGCCCAGTTCGTTTCAGTG	129	62

2. Materials and methods

2.1. Experimental protocol (GFP/CCl_4 model)

We developed a new in vivo model in which we could monitor the plasticity of BMCs into hepatocytes [12,16]. The mouse line C57BL6/Tg14 (act-EGFP) OsbY01 was a kind gift from Dr. Masaru Okabe (Genome Research Center, Osaka University, Osaka, Japan) [14]. C57BL/6 female mice were purchased from Japan SLC (Shizuoka, Japan). We injected 0.5 ml/kg body weight of CCl_4 into C57BL/6 mice at 6 weeks of age via the peritoneum twice a week for 4 weeks to induce persistent liver damage. At this time, the condition of recipient mice was liver cirrhosis. One day after 4 weeks of CCl_4 injection, 1×10^5 GFP-positive BMCs were injected slowly using a 31 G needle and Hamilton syringe via the tail vein. The mice that were injected with CCl_4 only were used as the control group. After BMC transplantation, the same dose of CCl_4 was injected twice a week. Individual mice were killed at 18 h after initial CCl_4 injection (2 days after BMC transplantation) and once a week after BMC transplantation for 4 weeks. All processes including surgical steps confirmed to the guidance of Yamaguchi University for animal and recombinant DNA experiments.

2.2. RNA preparation and microarray analysis

In both the BMC transplantation and control groups, the liver was excised 2 days and 1, 2, 3, and 4 weeks after transplantation. The mice were killed by cervical dislocation. The whole liver was removed and immediately frozen in liquid nitrogen. Liver samples were pooled at least two from whole liver of both mice groups (BMC transplantation and control CCl_4 damage at each points). Total RNA was isolated from pooled liver samples using an Atlas Glass Total RNA Isolation Kit (Clontech, Palo Alto, CA) [21]. Single strands of cDNA were synthesized using the primer mix, dNTP, aminoacryl dUTP, and MMLV-RT using an Atlas Glass Fluorescent Labeling Kit (Clontech). The synthesized cDNA probes were coupled to monoreactive Cy3 for fluorescent labeling. Probes were prepared in the same manner for the control group (no BMC transplantation) and BMC transplantaion group at the same time. The DNA microarray analysis was conducted using an Atlas Glass Mouse 1.0K Microarray System (Clontech) [22]. The above-mentioned cDNA probes were hybridized to a DNA chip composed of about 1100 DNA fragments by incubating the chip overnight at 50 °C with the probe. After incubation, the chip was washed using GlassHyb Wash Solution, RNase water and 20× SSC, rinsed with distilled water and then air dried. The signal intensity of each gene was measured using a fluorescent scanner (Axon Instruments, CA). The spot intensity of expression of each gene was assessed using the ArrayGauge System (Fuji Film, Tokyo, Japan). The raw data of the spot intesity were used for SOM analysis (All raw data of microarray are available at http://liver-project.med.yamaguchi-u.ac.jp/research/). We performed several analyses to obtain representative data.

2.3. SOM analysis for microarray

The microarray analysis showed that, of the 1100 genes on the DNA chips, although the expression of some genes was too small for further analysis, the expression data recorded of the remaining 1018 genes were sufficient for SOM data analysis. At each of five sampling times, i.e., 2 days and each week for 4 weeks, expression levels of 1018 genes for both control CCl_4 damage and BMC transplantation group were measured, respectively. To extract the genes that are differentially expressed before and after BMC transplantation, we defined the following equation (Fig. 1):

$$f_i(t) = \log_{10} \frac{y_i(t)}{x_i(t)}, \quad t = 1,2,3,4,5, \quad i = 1,2,\ldots,1018 \tag{1}$$

where $x_i(t)$ is the expression level of the control CCl_4 alone sample (CCl_4 alone without BMC transplantation) and $y_i(t)$ is the expression level of BMC transplantation sample for gene i (1,2,...,1018) at sampling point t, respectively. The term $f_i(t)$ represents the expression level of GFP/CCl_4 group normalized by the control group. If $y_i(t) = x_i(t)$, at that the value of $f_i(t)$, i.e., $\log_{10} 1$, was zero. By using this, we succeeded in extracting the change of gene expression by BMC transplantation. Point t shows time. t = 2d, 1w, 2w, 3w, and 4w showed 1, 2, 3, 4, and 5, respectively. To extract the change of gene expression with time, we followed the change of the values of $f_i(t+1) - f_i(t)$ with the increase in t. Using $f_i(t)$, we defined the 4-dimensional vector $F_i = [F_i(1), F_i(2), F_i(3), F_i(4)]^t$ for gene i, where

$$F_i(1) = f_i(2) - f_i(1)$$
$$F_i(2) = f_i(3) - f_i(2)$$
$$F_i(3) = f_i(4) - f_i(3)$$
$$F_i(4) = f_i(5) - f_i(4)$$

All genes were described and then used as input patterns for SOM analysis. SOM was performed using the SOM toolbox in MATLAB (The Mathworks Inc., Natick, MA; and http://www.cis.hut.fi/projects/somtoolbox/).

Each element of these vectors [Fi (i = 1,2,3,...,1018)] represents a chronological change of gene expression after BMC transplantation in GFP/CCl_4 model.

2.4. Reverse transcriptase (RT)-PCR analysis

Total RNA was isolated from the whole liver of both mice groups (BMC transplantation and control CCl_4 damage (n = 2, each group) using Isogen Total-RNA isolation kit (Nippon Gene Co., Ltd., Tokyo, Japan) at each of five sampling times, i.e., 2 days and each week for 4 weeks. These samples were obtained by independent experiments from microarray analysis. RT step was performed using SYBR RT-PCR kit (Takara Co., Tokyo, Japan).

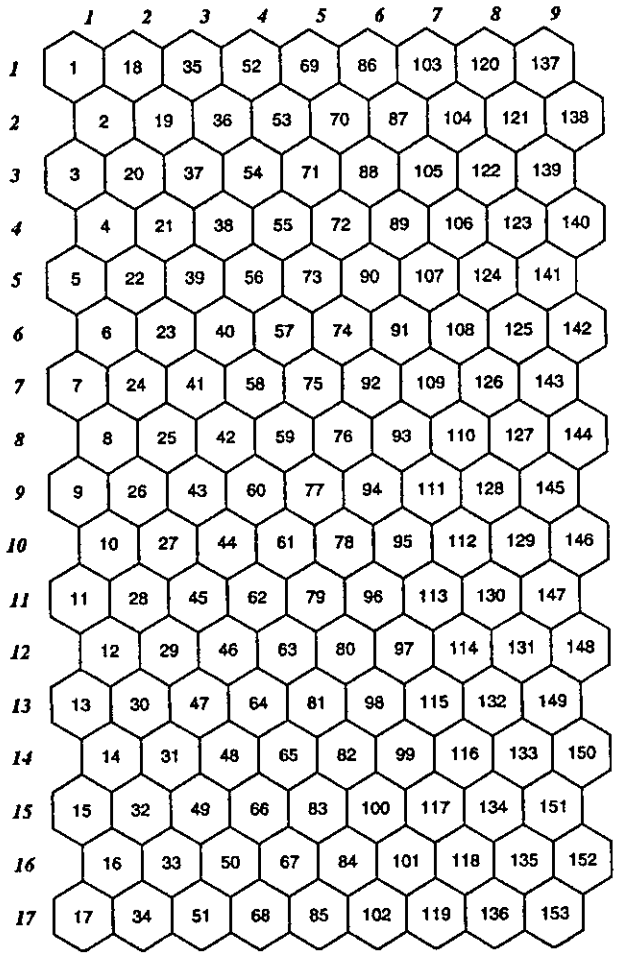

Fig. 2. The 1018 genes analyzed using microarray were divided into 153 clusters and arranged in a 17 × 9 matrix (height × width) of 153 hexagons (all raw data of microarray are available at http://liver-project.med.yamaguchi-u.ac.jp/research/). The number of genes varied among the clusters. Clusters with similar elements were arranged close to each other in the matrix.

Two μl of cDNA solution (100 ng of initial RNA) was amplified in 20 μl of reaction mixture containing 5 pmol of forward and reverse primer. PCR was performed for a total of 45 cycles, each of 95 °C for 5 s and 60 °C for 20 s [23]. We selected 13 genes to further clarify the difference expression pattern of each gene. c-kit, fibroblast growth factor (FGF)-6, matrix metalloproteinase (MMP)-2, MMP-9, tissue inhibitor of metalloproteinase (TIMP)-2, Hepatocyte growth factor (HGF), Numblike (NumbL) and homeobox (HOX) - D3, Glucose-6-phosphatase isomerase (GPI), vascular endothelial growth factor (VEGF), tumor necrosis factor receptor (TNFR)-1, hepatocyte nuclear factor (HNF)-4 and FGF-2 were selected. The primer used in this study is shown in Table 1. The relative ratio of each gene expression was determined referring with the mean expression level of control house keeping gene, glyceraldehyde-3-phosphate dehydrogenase (GAPDH) and 18 S ribosomal RNA expression.

2.5. SOM analysis compared between RT-PCR and microarray

To validate the results of SOM analysis depend on microarray, we compared SOM analysis between microarray and RT-PCR. We used the same equation and performed SOM analysis (Fig. 1) based on both the data of RT-PCR and microarray.

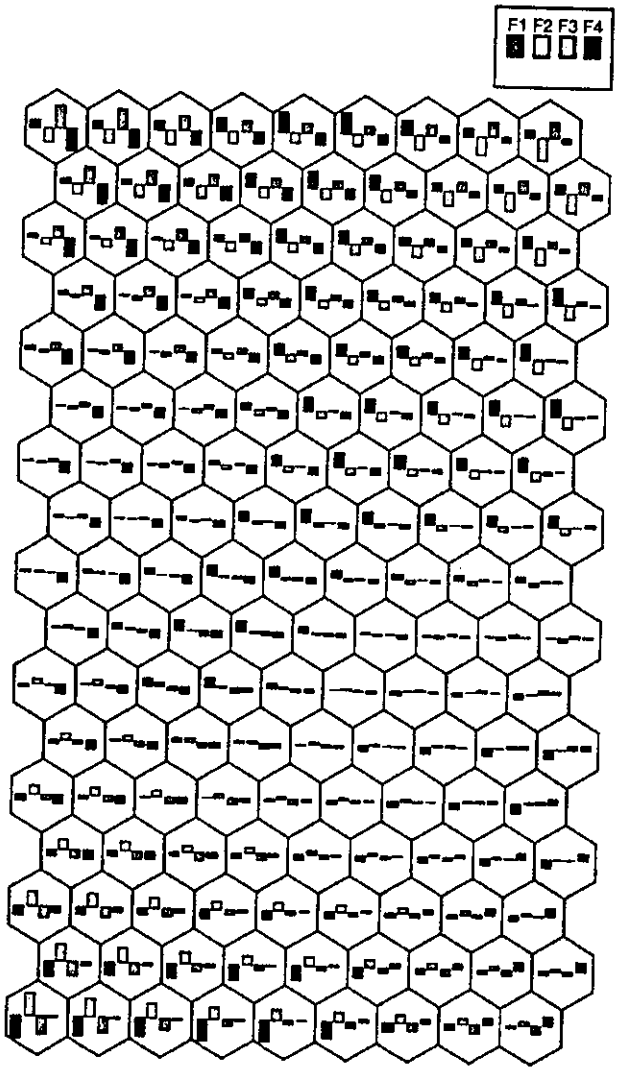

Fig. 3. The median value for gene expression for *F1*, *F2*, *F3*, and *F4* in each cluster is presented as a bar chart. As a reference, in cluster 1, the median value in *F1* and *F3* was increased, while that in *F2* and *F4* was decreased.

3. Results

The 1018 genes that could be analyzed by the DNA chips were classified into 153 clusters by SOM (Fig. 2). Genes in the same cluster showed similar gene expression pattern during the process of BMC trans-differentiation. On the SOM matrix, clusters with similar vector F_i elements (*F1*–*F4*) were arranged in close proximity to each other. Therefore, adjacent clusters on the matrix exhibited similar chronological changes in gene expression profiles during the process of plasticity of BMC into hepatocyte. Fig. 3 shows bar charts that represent the median value of gene expression for each cluster in *F1*, *F2*, *F3*, and *F4*. By analyzing each element (*F1*–*F4*) of vector *Fi*, the clusters were color coded to aid visualization of the SOM data (Fig. 4). For example, in the *F1* output, clusters 69, 70, and 86 containing upregulated genes in *F1* were colored dark brown. On the other hand, clusters with downregulated genes in *F1* were colored dark blue. The color bar on the right-hand side of the figure indicates the degree of gene expression from *F1* to *F4*, and a value of 0 indicates that there was little transient change in gene expression between the BMC transplantation and control CCl_4 injection groups. The following clusters exhibited marked changes in transient gene expression: in *F1*, clusters 69, 70, 86, 92, 125, 140, 141, 142, and 143; in *F2*, clusters 13, 14, 15, 16, 17, 32, 33, and 34; in *F3*, clusters 1, 2, 18, and 137; and in *F4*, clusters 118, 119, 133, 134, 135, 136, 148, 149, 150, 151, 152, and 153. To validate the data of SOM analysis based on microarray analysis, we performed SOM

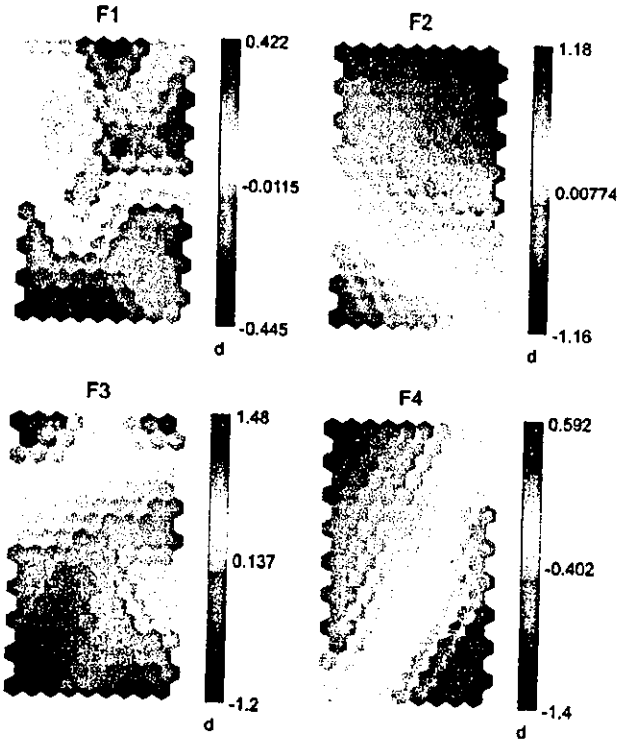

Fig. 4. The clusters were color-coded based on the median values for gene expression at the *F1*, *F2*, *F3*, and *F4* time periods. The color bar on the right hand side indicates the values in each period; dark brown for upregulated and dark blue for downregulated. A value of 0 indicates that there was little chronological change in gene expression between the transplantation and control groups.

analysis based on the data of RT-PCR for selected 13 genes using the same equation (Figs. 5A and B). Table 2 shows the list of genes in each cluster.

4. Discussion

By using specific equation to extract change of gene expression after BMC transplantation, we found that there were dramatic changes for both gene expression and distribution of gene clusters after BMC transplantation in GFP/CCl_4 model (Figs. 3 and 4). 1018 genes were classified into 153 patterns of change of gene expression using SOM analysis. These results might show that many genes had important reciprocal roles during the process of differentiation of BMC into albumin positive hepatocyte. To validate the SOM analysis based on microarray analysis, we performed SOM analysis based on selected 13 gene expressions analyzed by RT-PCR independently. c-kit, FGF6, MMP2, MMP9, and TIMP2 were selected from serious clusters at *F*1 periods (clusters 86, 92, and 125). HGF was selected from *F*2 periods (cluster 13). NumbL and HOXD3 were selected from *F*3 (cluster 1). GPI, VEGF, TNFR1, HNF4, and FGF2 were selected from *F*4 (clusters 136, 151, and 152). As shown in Fig. 5, we found the similar position of these selected genes. This means that the change of gene expression from microarray analysis is similar to that from RT-PCR analysis. These results showed the consistency of SOM analysis based on microarray using specific equation.

Cluster with color deeper than dark orange (69, 70, 125, 141, 142, and 143) showed the dramatic change in *F*1 period (Fig. 4). The c-kit gene, which was present in cluster 86, encodes a stem cell factor receptor which is related with rat hepatic stem cell, oval cell, activation [24]. FGF-6 was also extracted in cluster 86. FGF was known to have an important role of hepatocyte proliferation and liver development [25]. To focus on the change of *F*1 to *F*4 in cluster 86, we found that genes in cluster 86 were upregulated soon after BMC transplantation suggesting that the expression of these genes changes dynamically and might have an important role in the early stage of plasticity of BMC (Fig. 3). In cluster 125, genes involved in the regulation of liver fibrosis such as MMP2 and MMP9 were pointed out. These results were consistent with liver fibrosis recovered by BMC transplantation. MMP9 has been reported to facilitate the induction of hematopoietic cells from the marrow via the kit signal transduction pathway [26]. This result might suggest that ECM might be important for the

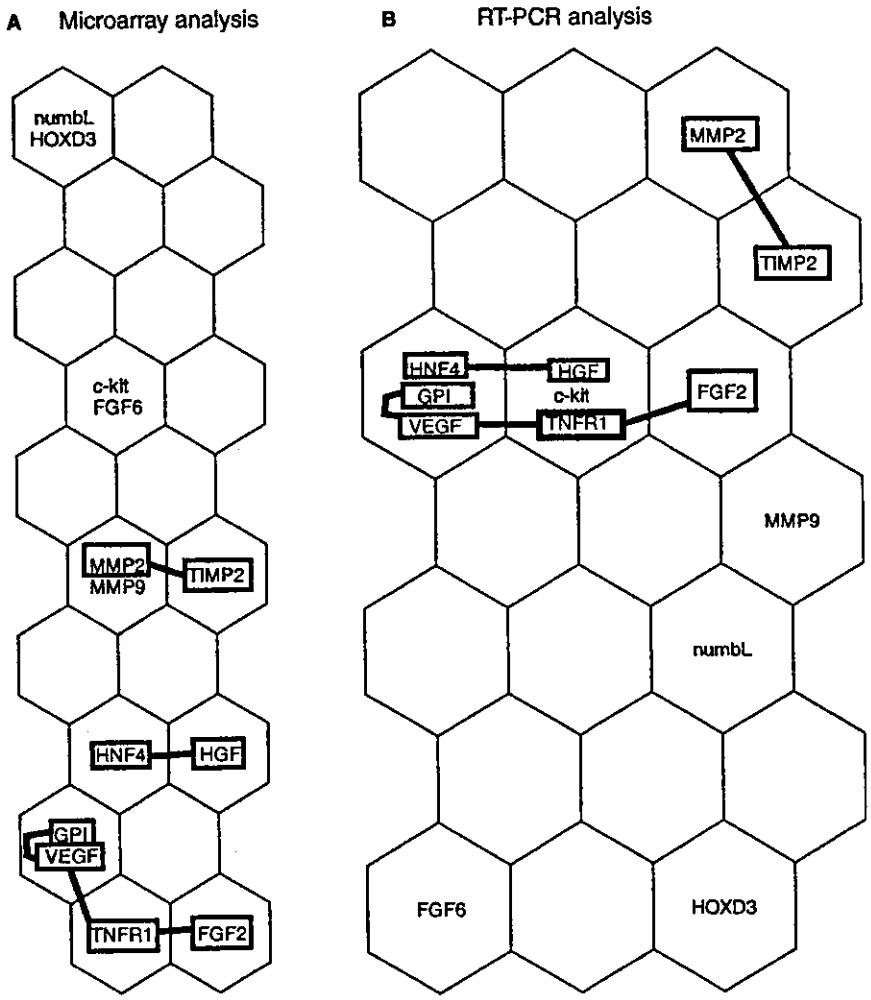

Fig. 5. For the genes, the data of microarray (A) and RT-PCR (B) were classified into clusters by SOM, respectively. Clusters with similar elements were arranged close to each other in the matrix.

Table 2
Selected *gene* grouped to clusters

Cluster No.	GenBank ID	Gene description
Clusters with remarkable variation of gene expression in F1		
86	U52951	Enhancer of zeste homolog 2 (EZH2); ENX1H
	X06368 X68932	Macrophage colony-stimulating factor 1 receptor (CSF1R) o-fms proto-oncogone
	Y00864 NM02099	c-kit proto-oncogene
	U14173	ski proto-oncogene
	M92415	Fibroblast growth factor 6 (FGF6)
69	X07439	Homeobox protein 3.1 (HOX3.1)
	X57487	Paired box protein 8 (PAX8)
	U43788	POU domain class 2-associating factor 1 (POU2AF1); OCT-binding factor 1 (OBF1); BOB1; OCA-B
	M84819	Retinoic acid receptor-γ (RXR-γ; RXRG)
	AF015848	E2F transcription factor 3 (E2F3)
	Z22649	mpl proto-oncogene; thrombopoietin receptor
	L27105	MOESIN-ezin-radin-like protein (MERLIN); schwannomin (SCH); neurofibromatosis 2(NF2)
	U51196	EB1 APC-binding protein
	Y00671	met proto-oncogene
	Z12604	Matrix metalloproteinase 11 (MMP11); stromelysin 3 (STMY3)
70	D90156	Myogenin (MYOG); myoD1-related protein
	U51037	CCCTC-binding factor (CTCF)
	U06119	Cathepsin H
142	J04946	Angiotensin-converting enzyme (ACE); dipeptidyl carboxypeptidase I (DCP1); kinase II
	U10551	Gem induced immediate early protein
	L34290	Transducin β-5 subunit GTP-binding protein G(i)/G(s)/G(t) β subunit 3
	M96653	Adenylate cyctase 6
	Z71173	Inositol 1,4,5-triphosphate receptor 2
	L76946	Phosphodiesterase 1C
	U12919	Adenylate cyclase type VII (AIP pyrophosphate-lyase) (adenylyl cyclase) (KTAA0037)
	D31788	BP3 alloantigen
	AA000715	S100 calcium-binding protein A1; S-100 protein α chain
	U97327	Calcylin binding protein
	U73004	Antileukoproteinase 1 (ALP1); secretory leukocyte protease inhibitor
140	U58992	Mothers against decapentaplegic homolog 1 (MADH1; mSMAD1); TGF-β signaling protein 1
	U36203	snoN: ski-related oncogene
	D17571	NADPH-cytochromc P450 reductase (CPR); POR
	U68058	Secreted frizzled-related protein 3 (SFRP3; mFIZ); frezzled
	U77638	Mothers against dpp homolog 5 (SMAD5; MADH5)
	M33385	Neurotrophic tyrosine kinase receptor type 2 (NTRK); tyrosine kinase receptor B (TRKB)
	X57277	ras-related C3 botulinum substrate 1 (RAC1)
	M21531	Calbindin-28K: calbindin 1 (CALB1)
	U53142	Nitric oxide synthase 3, endothelial cell
	U37775	Tuberin: TSC2 (tuberous sclerosis 2 protein)
	J05261	Lysosomal protective protein; cathepsin A; carboxypeptidase C (CPC); MO54
	M81591	Membrane metallo endopeptidase
	M14222	Cathepsin B (CTSB)
	X15475	Peripherin (PRPH)
141	U61969	Wingless-related MMTV integration site 10a protein (WNT10A)
	X76292	Desert hedgehog homolog (DHH); HHG3
	X67962	Interleukin 7 (IL7)
	X66196	Recoverin (RCV1; RCVRN); cancer-associated retinopathy protein (CAR protein), 23-kDa photoreceptor cell-specific protein
	U57311	14-3-3 protein η; protein kinase C inhibitor protein 1 (KCIP1); tyrosine 3-monooxygenase/tryptophan 5-monooxygenase activation protein η polypeptide (YWHAH)
	X16490	Macrophage plasminogen activator inhibitor 2 (PAI2; PLANH2)
	X05211	Laminin γ 1 subunit (LAMC1); laminin B2 subunit
125	U03421	Interleukin 11 (IL11)
	M84324	Matrix metalloproteinase 2 (MMP2)
	NM008610	
	X72795	Matrix metalloproteinase 9 (MMP9)
	NM013599	
	M59470	Cystatin C; cystatin 3 (CST3)

(*continued on next page*)

Table 2 (*continued*)

Cluster No.	GenBank ID	Gene description
143	U94350	Radical fringe homolog (RFNG)
	U37720	Cell division cycle 42 homolog (CDC42); 25-kDa GTP-binding protein (G25K)
	X73985	Calbindin 2 (CALB2); calretinin
	X61432	Calmodulin (CALM; CAM)
	U48853	ork-associated substrate (CRKAS; CAS)
	U24680	Dishevelled 2 homolog (DVL2)
	D00611	Basic immunoglobulin superfamily (BASIGIN; BSG); membrane glycoprotein 42 (GP42), neurothelin; CD147 antigen
	M28730	Tubulin β 4 (TUBB4)
	Z21848	DNA polymerase δ catalytic subunit (POLD1)
92	U37331	T-box protein 6 (TBX6)
	M61909	relA proto-oncogene; NF-κ-B transcription factor p65 subunit (NF-κB p65)
	U18542	Calcitonin receptor 1b
	U17985	Cannabinoid receptor 1 (CNR1; CBR), brain cannabinoid receptor
	U41285	Segment polarity protein dishevelled homolog 3 (DVL3), DSH homolog 3
	X62622	Tissue inhibitor of metalloproteinase 2 (TIMP2)
	NM011594	
	L07803	Thrombospondin 2 (THBS2; TSP2)
	X53929	Decorin (DCN); bone proteoglycan II (PG-S2), PG40
	X61435	Neuronal kinesin heavy chain (NKHC); KIF5C
	D10061	DNA topoisomerase I (*TopI*)
	D28492	Caspase 2 (CASP2); NEDD2 protein; ICH1 cysteine protease
	X66323	X-ray repair-complementing defective repair in Chinese hamster cells 5 (XRCO5)
Clusters with remarkable variation of gene expression in F2		
17	AF017085	BAP-135 homolog; DIWSIT; general transcription factor II-I (GTF2I)
	U77969	Neuronal PAS domain protein 2
	X97817	Semaphorin F(SEMAF)
	M84487	Vascular cell adhesion molecule 1 (VCAM1)
	M59378	Tumor necrosis factor receptor superfamily member 1B2 (TNFRSF1B2); tumor necrosis factor receptor 2 (TNFR2)
	U25995	Receptor (TNFRSF)-interacting serine-threonine protein kinase 1 (RIPK1; RIP)
	L22472	BCL2-associated X protein membrane isoform alpha (BAX-alpha)
	L33406	Uromodulin
	AF007268	Fibroblast growth factor 15 (FGF15)
	AF030433	Dickkopf homolog 1 (mDKK1)
	AF031896	Cerberus-related protein1 (CERR1)
	X58995	Calcium/calmodulin-dependent protein kinase IV catalytic subunit (CAM kinase-CR; CAMKIV;
34	D32132	Hairy and enhancer of split protein 5 (HES5)
	Z93947	Semaphorin H (SEMAH)
	U69535	Semaphorin J (SEMAJ)
	X97818	Semaphorin G (SEMAG); SEMA5B
	U25416	Tumor necrosis factor receptor superfamily member 8 (TNFRSF8); CD30L receptor
	U39643	fas-associated factor 1 (FAF1)
	Z22703	Fibroblast growth factor 7 (FGF7)
	X63615	Calcium/calmodulin-dependent protein kinase type II β subunit (CAM-kinase II β; CAMK-II β)
	U43187	Mitogen-activated protein kinase kinase kinase 3 (MAPKKK3; MAP3K3; MAPK/ERK kinase kinase 3 (MEK kinase 3; MEKK3)
	L35236	Mitogen-activated protein kinase 10 (MAP kinase 10 MAPK10; PRKM10); MAP kinase p49 3F12; Stress-activated o-jun N-terminal kinase 3 (JNK3); SAPK/ERK kinase 2 (SERK2)
	U03856	Receptor-type protein tyrosine phosphatase (PTPRCAP); C polypeptide-associated protein; CD45-Associated protein (C045-AP), LSM
16	L20331	Adenosine A3 receptor
	L41145	Bone morphogenetic protein 5 (BMP5)
	AB006787	Mitogen-activated protein kinase kinase kinase 5 (MAPKKK5; MAP3K5); MAPK/ERK kinase kinase S (MEKK5); apoptosis signar-regulating kinase 1 (ASK1)
	U92456	Serine/aninine-rich protein specific kinase 2 (SRPK2), WW domain binding protein 6 (WBP6)
15	X81579	Insulin-like growth factor-binding protein 1 (1GF-binding protein 1; K3FBP1)
	U60530	Mothers against decapentaplegic homolog 2 (MADH2; mSMAD2)
	AB005141	Klotho protein (KL)
	U77039	Four and a half LM domains 1 (FLH1); KyoT
51	Z32675	Hairless protein (HR)
	L10075	DNA-binding protein SMBP2
	S56660	Retinoic acid receptor β (RAR-β; RARB); nuclear receptor subfamily 1 group B member 2

Table 2 (*continued*)

Cluster No.	GenBank ID	Gene description
	X57413	Transforming growth factor β 2 (TQF-beta 2; TOFB2)
	M20473	cAMP-dependent protein kinase type I β regulatory chain (PRKAR1B)
	Y00703	Guanine nuclaotide-binding protein alpha stimulating activity potypeptide (GNAS)
32	Y07836	Stimulated by retinoic acid protein 14 (STRA14); STRA13; E47 interaction protein 1 (EIP1)
	X85993	Collapsin 1; semaphorin IIIA (SEMA3A), SEMAD
	L28177	Growth arrest and DNA damage-inducible protein (GADD45), DNA damage-inducible transcript 1
	L33768	Janus tyrosine-protein kinase 3 (JAK3)
	U07617	Growth factor receptor-bound protein 2 (GRB2); ASH protein
	L02526	Mitogen-activated protein kinase kinase 1 (MAP kinase kinase 1; MAPKK1; MAP2K1; PRKMK1); MAPK/ERK kinase 1 (MEK1)
	U66058	DNA ligase III; polydeoxyribonucleotide synthase (ATP) (DNL3)
	L28819	Involucrin (IVL)
33	X97052	Mitogen-activated protein kinase kinase 6 (MAP kinase kinase 6: MAPKK6; MAP2K6; PRKMK6); MAPK/ERK kinase 6 (MEK6); SAPKK3
	L09562	Protein-tyrosine phosphatase γ (R-PTP- γ; PTPRG)
	Z32767	DNA damage repair & recombination protein 52 homolog (RAD52)
14	X81466	Ephrin type A receptor 7 (eph receptor A7; EPHA7), embryonic brain receptor tyrosine kinase (EBK); developmental kinase 1 (mDK1)
	U37522	Tumor necrosis factor superfamily member 10 (TNFSFK 10); TNF-related apoptosis inducing ligand
	D38258	Fibroblast growth factor 9
	X77113	Growth differentiation factor 9 (GDF9)
	X06381	Leukemia inhibitory factor (LIF); cholinergic differentiation factor
	Z22532	Syndecan 1 (SYND1)
	M75716	Alpha-1-antitrypsin, 1-2 (AAT2), serine proteinase inhibitor 1-2 (SPI1-2); alpha 1 protease inhibitor 2; alpha-1- antiproteinase
	M64292	Anti-protiferative B-cell translocation gene 2 (BTG2); NGF- inducible protein TIS21
	L23971	Fragile X mental retardation syndrome 1 homolog (FMR1; FMRP)
13	U95610	NIMA-related protein kinase 2 (NEK2)
	U05252	Special AT-rich sequence-binding protein 1 (SATB1)
	U70017	Cyclin-D binding Myb-like protein (hDMPI)
	AF001287	Neural cell adhesion molecule 2 (NCAM2), olfactory axon cell adhesion molecule (OCAM)
	J04806	Osteopontin (OP); bone sialoprotein 1; minopontin; early T-lymphocyte activation 1 protein (ETA1); secreted phosphosprotein 1 (SPP1), calcium oxalate crystal growth inhibitor protein
	X83930	Cadherin 5 (CDH5); vascular epithelial cadherin (VE-cadherin)
	AF003747	Zinc transporter 4 (ZNT4)
	M16472	Myelin proteolipid protein (PLP). lipophilin; DM20
	XI5830	7B2 neuroendrocrine protein: secretogranin V (SGV; SCG5)
	X72307 NM010427	Hepatocyte growth factor (HGF)
	D84372	Non-receptor type II protein cyrosome, phosphocyrosome phosphrase
	M38700	ATP-dependent DNA helicase II 70-kDa subunit 70-kDa thyroid autoantigen; lupus Ku autoantigen protein p70 CTC box-binding factor 75-kDa subunit (CTCBF; CTC75)
cluster with remarkable variation of gene expression in F3		
1	UB6441 NM010950	numfaiike (numbL; m-nbl)
	M33158	CD3 antigen zeta (CD3Z)
	X04648	Low-affinity IgG Fc receptor II β (FCGR2B)
	D49658	LIM-homeodomain protein L3; LHX8
	L12705	Engrailed protein (En-2) homolog
	D49474	SRY-box containing gene 17 (SOX17)
	X73573	Homeobox protein D3 (HOXD3)
	NM010468	
	U62522	Sp4 zinc finger transcription factor
	U25096	Lung Kruppel like factor (LKLF)
	X90329	Lbx 1 transcription factor
	X61753	Heat shook factor 1
	U53925	Transcription factor C1
	U97076	FLICE-like inhibitory protein long form (FLIP-L)
18	M55S12	WT1; Wilms tumor protein; tumor suppressor
	M16449	Myeloblastosis prato-oncogene (MYB)
	X13945	Lung carcinoma myc-related oncogene 1 (L-myc; mycL1)
	M26391	Retinoblastoma-associated protein 1 (RB1); phosphoprotein 105 (PP105)
	U65594	Breast cancer type 2 susceptibility protein (BRCA2)
	U04807	FMS-like tyrosine kinase 3 ligand (FLT3L)
	M34563	T-ceB-specific surface glycoprotein CD28

(*continued on next page*)

Table 2 (*continued*)

Cluster No.	GenBank ID	Gene description
2	M32240	Peripheral myelin protein 22 (PMP22); CD25 antigen; SR13 myelin protein
	M63801	Gap junction alpha 1 protein (GJA1), connexin 43 (CXN43; CX43)
	AF013282	T-box protein 15 (TBX15); TBX14; TBX8
	U63386	Early development regulator 1 (EDRI); pdyhomeotic 1 homolog (mPHI)
	J05154	Lecithin cholesterol acyltransferase (LCAT); phosphatidylcholine sterot acyltransferase; phospholipid cholesterol acyftransferase
137	M55171	Rhodopsin (RHO), opsin (mOPS)
	D50311	Myocyte enhancer factor 2B (MEF2B)
	X14943	Contactin 1 (CNTN1); F3 neuronal cell adhesion molecule (F3CAM)
	U12570	von Hippel-Lindau syndrome homolog (VHLH)
	V00727	fos proto-oncogene
	U36799	retinoblastoma- like protein 2 (RSL2); retinoblastoma-relatad protein PRB2/p130
	S59388	Erythropoietin receptor (EPOR)
	Z31683	activin A receptor type 1B
	S53216	Tyrosine-protein kinase ryk; kinase vik; nyk-R
	AF039601	TGF-bttta receptor type IB (betaglycan); candidate tumor suppressor gene
	X06203	Interleukin 8 (IL6)
Clusters with remarkable variation of gene expression in F4		
152	L12140	Groucho gene-related protein (GRG); amino enhancer of split protein (AES)
	M98502	Zinc finger protein 46
	S79463	Semaphorin I (SEMAI)
	X91144	P-selectin glycoprotein ligand 1 (PSGL1: SELPLG; SELP1)
	U04294	Electocardiographic QT syndrome 2 potassium channel subunit
	M14220	Glucose-6-phosphate isomerase (GPI)
	NM008155	
	M95200	Vascular endothelial growth factor (VEGF)
	NM009505	
	M30643	Heparin-fainding growth factor 5 (HBGF5); fibroblast growth factor 5 (FGF5)
	U51866 U17112	Casein kinase II alpha 1 related sequence 4 (CSNK2A1-RS4)
	U67916	Dentin sialophosphoprotein (DSPP)
	U49739	Unconventional myosin VI
153	S663B5	CREB-binding protein
	X85994	Semaphorin IIIC (SEMA3C); SEMAE
	U28724	Postmeiotic segregation increased 2 homolog (PMS2)
135	X12875	Neural cell adhesion molecule LI (N-CAM LI; LtCAM; CAML1)
	L24755	Bone morphogenetic protein 1 (BMP1)
	X83106	MAX dimerization protein (MAD)
	U34960	Transducin beta-2 subunit
	D86726	MCM6 DMA replication licensing factor (P105MCM)
136	D31967	Jumonji protein
	U59496	Hypoxia inducible factor 1 alpha subunit (HIF1-alpha; HIF1A); ARNT-interactmg protein
	X85992	Somaphorin C (SEMAC)
	X07640	Cell surface glycoprotein MAC-1 alpha subunit; CR-3 alpha subunit; GD11B antigen; leukocyte adhesion receptor MO1; integrin alpha-M (ITGAM)
	X57796	Tumor necrosis factor receptor 1 (TNFR1)
	NM011609	
	X53798	Small inducible cytokine subfampy B member 2 (SCYB2); macrophage inflamatory protein 2 (M1P2)
	X78850	Mitogen actived kinase-activated protein kinase 2 (MAPKAP kinase 2; MAPKAPK2); 60-kDa ribosomal protein S6 kinase potypeptide 1 (RPS6KC1)
	U43144	Phospholipase C β 3 (PLC-β 3; PLCB3)
	X83536	Matrix metalloproteinase 14 (MMP14): membrane-type matrix matatoproteinase 1 (MTMMP1)
	Y13602	Filensin, beaded filament structural protein in lens 1 (BFSP1)
150	AF033011	distal-less homeobox protein 5 (DLX5)
	D63644	Aryl hydrocarbon receptor nuclear translocator 2 (ARNT2)
	S70632 S70756	
	S70629	T-cell leukemia homeobox 1 (TLX1); homeobox protein 11 (HOX11)
	S81932	distal-less homeobox protein 3 (DLX3)
	X75330	Drosophila NK5 transcription factor-related locus 1 (NKX-5.1), H6 homeobox protein 3 (HMX3)
	U89487 U89489	LIM homeobox protein cofactor 1A (CUM1A); CUM1B; LIM domain-binding protein 3 (LDB3)
	U36340	CACCC-box-binding protein basic Kruppel like factor (BKLF): Kruppel-like factor 3 (KLF3)
	U42554	Single-minded 2 (SIM2)
	U33626	Promyelocytic leukemia gene (PML)

Table 2 (*continued*)

Cluster No.	GenBank ID	Gene description
	X56135	Prothymosin alpha (PTMA)
	U43512	Dystroglycan 1
	M13071	A-raf proto-oncogene
	M36829	Heat shock 84-kDa protein 1 (HSP84-1); HSP90
	M89802	Wingless-related MMTV integration site 7b protein (WNT7B)
	M30903	B-lymphocyte kinase (BLX)
	U43298	Laminin β 3 subunit (LAMB3); kalinin B1 subunit
151	D29015	Hepatic nuclear factor 4-alpha (HNF4-alpha)
	NM008281	
	M31042	Immediate early response protein 2 (IER2); T-lymphocyte activated protein; cyclo-heximide-induced Protein 1 (CHX1)
	U43900	STAM; signal transducing adaptor molecule
	M13177	Transforming growth factor β 1 (TGF-β 1; TGFB1)
	M30644	Fibroblast growth factor 2 (FGF2)
	NM008006	
	M76601	Cardiac myosin heavy subunit alpha isoform (MYH6; MYHCA)
148	AB009453	Transcription factor 21 (TCF21); basic helix-loop-helix factor COR1; POD1
	S71659	LIM homeobox protein 4 (LHX4); GSH4
	S79041	Genomic screened homeobox protein 2 (GSH2)
	U58533	est2 repressor factor (ERF)
	J03770	Homeobox protein D4 (HOXD4); HOX4.2; HOX5.1
	X59252	Homeobox protein 8 (HOX8)
	J03168	Interferon regulatory factor 2 (IRF2)
	S68108	Brahma-related protein 1 (BRG1); swi/snf-related matrix-associated actin dependent regulator of chromatin subfamily a member 4 (SMARCA4)
	D78382	Transducer of erbB2 (TROB; TOB)
	X59421	Fli-1 ets-related proto-oncogene
	M62860	Myelin protein zero
	D31942	Oncostatin M (OSM)
	M29464	Platelet-derived growth factor A subunit (PDGFA; POGF1)
	M69042	PKC-δ; protein kinase C δ type
	U29539	Retinoic acid-inducible E3 protein; stimulated by retinoic acid 13 (STRA13), hematopoetic-specific Protein E3; orfB
	U26967	Cordon-bleu protein (COBL)
149	L38248	LIM homeobox protein 3 (LHX3; UM3)
	X56230	Octamer-binding transcription factor 1 (OCT1; OTF1); NF-A1; POU domain class 2 transcription factor 1 (POU2F1)
	X13721	Homeobox protein 2.4 (HOX2.4)
	L04662	γ-Aminobutyric acid transporter 4 (GABA-A transporter 4; GABT4)
	U59746	B-cell lymphoma protein W (BCLW); BCL2-like protein 2 (BCL2L2)
	M16819	Lymphotoxin alpha (LTA), tumor necrosis factor β (TNF-β; TNFB)
	U12147	Laminin alpha 2 subunit (LAMA2). dystrophia muscularis protein (DV); merosin heavy chain; laminin M subunit
	U22421	Leptin (LEP); obese factor (OB)
133	D10329	CD7 antigen
	D86603	btb and cnc homolog 1 (BACH1)
	U36384	Dermis expressed 1 protein (DERM01)
	M58633	P58/GTA; galactosy transferase associated protein kinase (cdc2-related protein kinase)
	D83698	Activator of apoptosis harakiri (HRK); neuronal death protein 5 (DP5); BID3
	L08235	Clusterin (CLU); clustrin; apolipoprotein J (APOJ); sulfated glycoprotein 2 (SGP2; mSGP2)
	X07414	DNA excision repair protein ERCC1
134	U61155	LIM homeobox protein 2 (LIM2); LHX5
	U20553	p57kip2; cdk-inhibitor kip2 (cyclin-dependent kinase inhibitor 1 B); member of the p21CP1 Cdk inhibitor family; candidate tumor suppressor gene
	U05671	Adenosine At receptor (ADORA1)
	L37663	Acetylcholine receptor alpha 7 neural
	M97017	Bone morphogenetic protein 8A (BMP8A), ostoogenic protein 2 (OPS)
	AF027503	guanylate kinase membrane-associated inverted protein 1 (GUKMI1; MAGI-1)
	M84817	Retinoid X receptor alpha (RXR-aJpha; RXRA)
	J03520	Tissue plasminogen activator (T-plasminogon activator PLAT; TPA)
118	X99063	Zyxin(ZYX)
	X14194	Nidogen (NID); entactin (ENT)
119	Y15001	Iroquois-related homeobox protein 3 (IRX3)
	Z23066	Microphthalmia-associated transcription factor (MITF; MI); microphthaltmia-related protein
	X73360	Transducin-like enhancer of split protein 3 (TLE3; ESG)

(*continued on next page*)

Table 2 (*continued*)

Cluster No.	GenBank ID	Gene description
	U65091	Melanocyte-specific gene 1 (MSG1); Cbp/p300-interacting transactivator with Glu/Asp-rich carboxy-terminal domain 1 (CITED1)
	X97986	Desmocollin 1A/1B (DSC1)
	U81317	Myelin-associated oligodendrocytic basic protein
	U21050	TNF receptor-associated factor 3 (TRAF3); TRAFAMN; C040 receptor-associated factor 1 (CRAF1)
	D83966	Protein tyrosine phosphatase
	L19622	Tissue inhibitor of metalloproteinase 3 (TIMP3); SUN
	AF021031	DiGeorge syndrome chromosome region 6 protein (DGCR6)

plasticity of BMC. In the *F2* time period, clusters 13, 14, 15, 16, 17, 32, 33, and 51 were dramatically changed. In cluster 13, hepatocyte growth factor (HGF) was discovered. HGF is involved in hepatocyte proliferation [27,28]. HGF might also have an important role in GFP/CCl_4 model. In the *F3* time period, clusters 1, 2, 18, and 137 were focused. NumbL is involved in asymmetric division of nerve precursor cells [29]. The HOXD3 genes encode information important for determining the positional relationships of the antero-posterior axis in embryogenesis [30]. NumbL and HOXD3 might have an important role in regulating the plasticity of BMC. In *F4*, clusters 118, 119, 133, 134, 135, 136, 148, 149, 150, 151, 152, and 153 were found. In this period, genes involved in hepatocyte differentiation and homeostasis, such as GPI and HNF4, were focused [31]. This enzyme is essential for the glycolytic metabolism of hepatocytes. In the GFP/CCl_4 model, the level of albumin in bone marrow-derived hepatocytes increased significantly [12]. The fact that an enzyme such as GPI was induced at this period suggests that, at 4 weeks after BMC transplantation, transplanted BMCs begin to possess some of the metabolic functions of hepatocytes. HNF4-α was also upregulated in *F4* period. HNF4 plays an important role in the metabolic regulation of hepatocytes [32,33]. These results might be related with BMC differentiated into functional hepatocyte at this period in GFP/CCl_4 model. VEGF was also upregulated. VEGF promotes vasculogenesis and liver regeneration [34]. VEGF might also have an important role in accelerating the liver regeneration in GFP/CCl_4 model. Gene involved in inflammation such as TNF-R1 was also pointed out in GFP/CCl_4 model. TNF-alpha related inflammation signal is important in the generation of hepatoblast [17]. These results also showed that TNF-α related signal might be important for plasticity of BMC in GFP/CCl_4 model.

Here, we analyzed the change of molecular signature after BMC transplantation in GFP/CCl_4 model in mRNA level. Still many precise things are unconfirmed, but we think the information is useful to understand the mechanism of the plasticity of BMC in GFP/CCl_4 model. In the future, we are planning to further analyze the mechanisms.

Acknowledgements: We thank Dr. Masaru Okabe (Genome Research Center, Osaka University) for the gift of GFP transgenic mice and Mr. Jun Oba for valuable technical support.

References

[1] Alison, M.R. et al. (2000) Nature 406, 257.
[2] Petersen, B.E. et al. (1999) Science 284, 1168–1170.
[3] Theise, N.D., Nimmakayalu, M., Gardner, R., Illei, P.B., Morgan, G., Teperman, L., Henegariu, O. and Krause, D.S. (2000) Hepatology 32, 11–16.
[4] Terada, N. et al. (2002) Nature 416, 542–545.
[5] Ying, Q.L., Nichols, J., Evans, E.P. and Smith, A.G. (2002) Nature 416, 545–548.
[6] Hakelien, A.M. and Collas, P. (2002) Cloning Stem Cells 4, 379–387.
[7] Krause, D.S., Theise, N.D., Collector, M.I., Henegariu, O., Hwang, S., Gardner, R., Neutzel, S. and Sharkis, S.J. (2001) Cell 105, 369–377.
[8] Ianus, A., Holz, G.G., Theise, N.D. and Hussain, M.A. (2003) J. Clin. Invest. 111, 843–850.
[9] Stamm, C. et al. (2003) Lancet 361, 45–46.
[10] Hamano, K., Li, T.S., Kobayashi, T., Hirata, K., Yano, M., Kohno, M. and Matsuzaki, M. (2002) Ann. Thorac. Surg. 73, 1210–1215.
[11] Terai, S., Yamaoto, N., Omori, K., Sakaida, I. and Okita, K. (2002) J. Gastroenterol. 37, 162–163.
[12] Terai, S. et al. (2003) J. Biochem. (Tokyo) 134, 551–558.
[13] McTaggart, R.A. and Feng, S. (2004) Hepatology 39, 1143–1146.
[14] Okabe, M., Ikawa, M., Kominami, K., Nakanishi, T. and Nishimune, Y. (1997) FEBS Lett. 407, 313–319.
[15] Shinoda, K., Mori, S., Ohtsuki, T. and Osawa, Y. (1992) J. Comp. Neurol. 322, 360–376.
[16] Yamamoto, N. et al. (2004) Biochem. Biophys. Res. Commun. 313, 1110–1118.
[17] Watanabe, T. et al. (2002) Dev. Biol. 250, 332–347.
[18] Sakaida, I., Terai, S., Yamamoto, N., Aoyama, K., Ishikawa, T., Nishina, H. and Okita, K. (2004). Hepatology (in press).
[19] Schena, M., Shalon, D., Davis, R.W. and Brown, P.O. (1995) Science 270, 467–470.
[20] Xiao, L., Wang, K., Teng, Y. and Zhang, J. (2003) FEBS Lett. 538, 117–124.
[21] Quaglino, E. et al. (2004) J. Clin. Invest. 113, 709–717.
[22] Ishigaki, S. et al. (2002) FEBS Lett. 531, 354–358.
[23] Nagata, M. et al. (2003) Int. J. Cancer 106, 683–689.
[24] Fujio, K., Evarts, R.P., Hu, Z., Marsden, E.R. and Thorgeirsson, S.S. (1994) Lab. Invest. 70, 511–516.
[25] Zaret, K.S. (2000) Mech. Dev. 92, 83–88.
[26] Heissig, B. et al. (2002) Cell 109, 625–637.
[27] Nakamura, T., Nishizawa, T., Hagiya, M., Seki, T., Shimonishi, M., Sugimura, A., Tashiro, K. and Shimizu, S. (1989) Nature 342, 440–443.
[28] Miyazawa, K. et al. (1989) Biochem. Biophys. Res. Commun. 163, 967–973.
[29] Zhong, W., Feder, J.N., Jiang, M.M., Jan, L.Y. and Jan, Y.N. (1996) Neuron 17, 43–53.
[30] McGinnis, W. (1994) Genetics 137, 607–611.
[31] Massillon, D., Arinze, I.J., Xu, C. and Bone, F. (2003) J. Biol. Chem. 278, 40694–40701.
[32] Li, J., Ning, G. and Duncan, S.A. (2000) Genes Dev. 14, 464–474.
[33] Kamiya, A., Inoue, Y. and Gonzalez, F.J. (2003) Hepatology 37, 1375–1384.
[34] Redaelli, C.A., Semela, D., Carrick, F.E., Ledermann, M., Candinas, D., Sauter, B. and Dufour, J.F. (2004) J. Hepatol. 40, 305–312.

Down-regulation of matrix-invasive potential of human liver cancer cells by type I interferon and a histone deacetylase inhibitor sodium butyrate

FUMIHIKO KANEKO[1,2], HIDETSUGU SAITO[1], YOSHIMASA SAITO[1], KANJI WAKABAYASHI[1], NOBUHIRO NAKAMOTO[1], SHINICHIRO TADA[1], HIDEKAZU SUZUKI[1], SATOSHI TSUNEMATSU[2], NAOKI KUMAGAI[2] and HIROMASA ISHII[1]

[1]Department of Internal Medicine, School of Medicine, Keio University, 35 Shinanomachi, Shinjuku-ku, Tokyo 160-8582; [2]Liver Center, Department of Internal Medicine, Kitasato Institute Hospital, 5-9-1 Shirokane, Minato-ku, Tokyo 108-8642, Japan

Received November 3, 2003; Accepted December 17, 2003

Abstract. We have demonstrated anti-proliferation and anti-metastasis effects of both interferon-α and a histone deacetylase inhibitor, sodium butyrate, on human liver cancer cell lines. In this study, invasive ability of human liver cancer cell lines through the matrix-coated membrane was examined and inhibitory effect of interferon-α and sodium butyrate was investigated. Among six human liver cancer cell lines, HLE and HLF showed high invasive ability using the Matrigel invasion assay. This invasion ability was significantly inhibited by pretreatment of the cells with 1000 IU/ml of interferon-α or 2 mM of sodium butyrate. Gelatin zymography and the matrix metalloproteinase-2 and -9 activity assay showed that these two cell lines produce active- and pro-matrix metalloproteinase-2 and -9, and their activity was significantly reduced by pretreatment with both agents. Real-time quantitative reverse transcription-polymerase chain reaction showed decrease in matrix metalloproteinase-1 mRNA levels by pretreatment with both agents, but mRNA levels of tissue inhibitor of matrix metalloproteinase-1 and -2 were differently modulated by interferon-α and sodium butyrate. These results suggest that interferon-α and sodium butyrate reduce a chance of invasion and metastasis of human liver cancer cells by inhibiting matrix metalloproteinase activity, although its inhibitor is differently regulated.

Correspondence to: Dr Hidetsugu Saito, Department of Internal Medicine, School of Medicine, Keio University, 35 Shinanomachi, Shinjuku-ku, Tokyo 160-8582, Japan
E-mail: hsaito@sc.itc.keio.ac.jp

Key words: invasion, matrix metalloproteinase, hepatocellular carcinoma, type I interferon, sodium butyrate

Introduction

Human hepatocellular carcinoma (HCC) is one of the malignant tumors prevalent world-wide. The number of patients with HCC is still increasing in Japan, especially that caused by chronic hepatitis C virus (HCV) infection. The incidence of HCC is higher in patients with chronic hepatitis C than in those with chronic hepatitis B and non-B, non-C including alcoholic (1). Epidemiological data suggest that there is a close correlation between duration of chronic HCV infection and incidence of hepatocarcinogenesis. HCV is a ribonucleic acid (RNA) virus that is not reverse transcribed to deoxynucleic acid (DNA), and this virus does not invade into the nuclei and never achieve integration to host DNA. This virus by itself does not explain the molecular mechanism of hepatocarcinogenesis in chronic HCV infection. Genomic instability caused by HCV-related chronic inflammation may be the most important event in HCV-related carcinogenesis (2), because it takes a long time for development of HCC after initial infection of HCV and recent studies revealed that the relationship between duration of the infection, fibrosis of the liver, and HCC occurrence rate is very close (3,4), and moreover elimination of HCV resulted in reduction of HCC occurrence rate after then (5). Thus, the liver with chronic HCV infection is considered to be in a hypercarcinogenic state, the state in which genes are prone to mutation (6).

In such a hypercarcinogenic state, HCC develops all around the liver whether or not multiple HCC develops at the same time or at the different time, resulting in frequent recurrence of HCC after hepatic resection has occurred in the different regions (4). Since the high-risk situation of HCC development has been defined and we closely followed up the patients by the ultra sound and other diagnostic examinations, we can detect small HCC, <2 cm diameter. These observations, that the frequent recurrence of HCC and the detection of small HCC, lead hepatologists to treat HCC with local ablation modalities, such as percutaneous ethanol injection, microwave coagulation therapy, and radio

frequency ablation (7), unless liver transplantation is indicated. In advanced cases, transarterial chemo-embolization (TACE) is another effective therapeutic modality (8,9). These various therapeutic procedures have decreased death rate of this disease, but it is still insufficient and we have no sufficiently effective therapy for its metastasis to other organs. Recently chemo-adjuvant therapy using type I interferon (IFN) has been introduced and is shown to be effective in advanced cases (10-12). However, the contribution of this treatment to life expansion is still under investigation (13).

We have studied the chemopreventive effect of differentiation inducers for human HCC cells (14). Among them, type I IFN and sodium butyrate, one of histone deacetylase (HDAC) inhibitors, were the most effective agents (15). Type I IFN can induce apoptosis of human HCC cells (16), and if the cell is not sensitive for apoptosis (17), cell cycle arrest is induced by IFN, resulting in reduction of cell proliferation and decrease in malignant phenotypes, probably according to the genomic polymorphisms (18,19). On the other hand, butyrate is a 4-carbon short fatty acid, which is a fermented product, and an HDAC inhibitor, which changes genomic transcription epigenetically. Recent studies showed that epigenetic changes such as DNA methylation in CpG islands of some oncogenes and histone acetylation are important in hepatocarcinogenesis (20).

These two agents, IFN and butyrate, similarly reduced HCC cell proliferation with increase in albumin production and decrease in α-fetoprotein production (15,21). These also similarly reduced c-myc expression (22,23), telomerase activity (24), and a metastasis potential of HCC cells by increasing expression of cell-cell adhesion molecules E-cadherin and ß-catenin (25). Thus, these two agents may affect another malignant potential of HCC, invasion ability, but little is known about this characteristic so far. It was demonstrated that human HCC cells require matrix metallo-proteinases (MMP) activity for migration and invasion (26). In the present study, to investigate the effect of type I IFN and sodium butyrate on invasive potential of human HCC cells, the matrix-coated gel invasion assay was performed and effect of IFN and butyrate on the production of MMP-1, -2 and -9 or tissue inhibitor of MMP (TIMP)-1 and 2 from HCC cells were examined. Thus, we investigated possible chemopreventive effect of the agent and its mechanisms in human HCC.

Materials and methods

Cells. Human HCC cell lines, HLE, HLF (27), HepG2, PLC/PRF/5, HCC-T (28) and HCC-M (29) were used in this study as described elsewhere (30). HCC-T and HCC-M were cultured in RPMI-1640 (Nissui Seiyaku, Tokyo, Japan) supplemented with 10% fetal bovine serum (Gibco, Grand Island, NY), 100 IU/ml of penicillin (Gibco) and 100 µg/ml of streptomycin (Gibco). HLE, HLF, HepG2 and PLC/PRF/5 were cultured in Eagle's modified essential medium (Nissui Seiyaku) supplemented with the same agents. These cells were cultured at 37˚C in the 5% CO_2 incubator and the medium was changed every two days.

Detection of apoptosis. To confirm that the treated cells were not dead, we observed morphologic aspect of the cell and further performed terminal deoxynucleotide transferase-mediated dUTP nick end-labeling (TUNEL) assay in the same experimental condition. The procedure of TUNEL assay has already been described (31).

Cell mobility assay. Since cell mobility is concerned to cancer cell invasion and metastasis, we tried to quantitatively measure the cell mobility and evaluate the effect of IFN-α and sodium butyrate using an inverted phase-contrast microscope (Nikon TMD300, Nikon, Tokyo, Japan) equipped with a digital time-lapse image analyzing system (Aquacosmos, version 2.0, Hamamatsu Photonics, Hamamatsu, Japan). The image of the cell was digitally recorded before the application of the test drug (0 h) and every 30 min after the start of the test drug for 2 days under the cell culture conditions. Collected 97 digital images were analyzed by a digital image analyzer.

Matrigel invasion assay. In vitro invasive potential of cancer cells was assayed using the Biocoat Matrigel Invasion Chamber (32) (Becton Dickinson Labware, Bedford, MA). Human HCC cells ($5x10^4$) were seeded onto the upper chamber of double-structured matrix gel chamber with 1% bovine serum albumin (BSA, Sigma-Aldrich Japan K.K., Tokyo, Japan) and the conditioned culture supernatant of NIH/3T3 cells, which was obtained from serum-free culture, was added to the lower chamber as a chemo-attractant. In this assay system, the cancer cells dissolve the matrix gel consisting of laminin, collagen type IV, heparan sulfate, proteoglycan, entactin and invade into 8 µm small holes, and appear on the lower surface of the membrane. The cells were cultured in this matrix gel chamber at 37˚C for 24 h in a CO_2 incubator and were fixed with 100% methanol and Giemsa stained. The cells on the upper portion of the matrix membrane were wiped off with cotton tips and cells on the other side of this membrane were observed by a phase-contrast microscopy. Number of invaded cells was counted in randomly selected 5 observation fields in a membrane at 100-fold magnification.

Treatment of HCC cell lines with IFN-α and sodium butyrate. Cancer cells were cultured in culture disks with natural IFN-α (Sumiferon®, Sumitomo Pharmaceutical Co., Osaka, Japan) at $1x10^2$ IU/ml and $1x10^3$ IU/ml or 2 mM of sodium butyrate (Sigma-Aldrich Japan) for 7 days. The medium was changed every 2 days. We selected the dose of sodium butyrate according to our preliminary experiments, which showed that 2 mM concentration of sodium butyrate induced HCC cells to significant reduction of their proliferation without inducing apoptosis. In some cell lines, increase in albumin production and reduction of α-fetoprotein production was induced in this concentration.

Gelatin zymography. HLE and HLF cells were cultured as described above with and without IFN or sodium butyrate for 7 days until the culture disk became confluent. The cells were recovered and washed 3 times with PBS and further cultured in serum-free medium for 48 h, and then the culture supernatant was obtained. The culture supernatant was concentrated with Centricon-10 (Millipore Co., Billerica,

MA) to 10-fold concentration, and this concentrated medium was used as the conditioned medium. The protein concentration in each medium was determined using the Bio-Rad DC protein assay kit (Bio-Rad Laboratories, Hercules, CA). Gelatinase activity in the conditioned medium was assessed by gelatin zymography following the methods described elsewhere (33). The conditioned medium which contained equal amounts of protein (10 µg) and the same volume of sample buffer (0.3 M Tris-HCl pH 6.8, 40% glycerol, 2% (w/v) SDS, 0.1% bromophenol blue) was mixed and incubated at 37°C for 30 min. The sample was electrophoresed on 9% SDS polyacrylamid gel containing 1% gelatin at 4°C at 30 mA. The gel was washed with 2.5% Triton X-100 twice and was incubated at 37°C for 15-18 h in TNC (50 mM Tris-HCl pH 7.5, 0.15 M NaCl, 10 mM $CaCl_2$) and was stained with Coomassie brilliant blue-R, followed by destaining with 5% isopropanol and 8% acetic acid.

Matrix metalloproteinase -2, and -9 activity assay. To investigate the mechanism of matrigel invasion and the effect of IFN and sodium butyrate, active form of MMP-2 and 9 was measured by the matrix metalloproteinase-2, and -9 activity assay system (34) (Amersham Bioscience Corp., Piscataway, NJ). The culture supernatant was obtained according to the procedure described above and was diluted 10-fold. This conditioned supernatant was applied to the measurement system. The procedure was achieved according to the instructions supplied by the manufacturer. The assay uses the pro-form of a detection enzyme that can be activated by capturing active MMP-2 or -9 and changes into an active detection enzyme. The MMP-activated detection enzyme was quantitatively measured using a specific chromogenic peptide substrate. The resultant color was read at 405 nm in a microtiter plate spectrophotometer. The concentration of active MMP-2 or -9 in the conditioned medium was determined by interpolation from a standard curve.

Effect of IFN and butyrate on the expression of MMP-1 and TIMP-1, -2. RNA was extracted from cancer cells with a modified acid guanidinium thiocyanate-phenol-chloroform method using Isogen (Nippon gene Co., Tokyo, Japan).

cDNA was synthesized from 5 µg of mRNA using ProSTAR™ First-Strand RT-PCR Kit (Stratagene, La Jolla, CA). The procedure was achieved according to the instructions supplied by the manufacturer. cDNA was labeled with SYBR Green during PCR (1 µl cDNA, 2X SYBR Green PCR Master Mix, each 5 pmol/µl of forward and backward primers; total 50 µl). PCR was performed and the products were detected using ABI PRISM 7700 detection system (Applied Biosystem, Foster City, CA). Reaction started at 50°C for 2 min and at 95°C for 10 min, and then 95°C 15 sec and 60°C 1 min for 40 cycles. A human fibrosarcoma-derived cell line HT-1080 was used as a calibration sample, and expression of glyceraldehydes-3-phosphate dehydrogenase (GAPDH) mRNA was used as an internal control. The primers used in this study were as follows: MMP-1 (35): forward, 5-CGG-TTT-TTC-AAA-GGG-AAT-AAG-TAC-T-3 (1092-2016); reverse, 5-TCA-GAA-AGA-GCA-GCA-TCGA TATG-3 (1219-1197); TIMP-1 (36): forward, 5-TGC-CGC-ATC-GCC-GAG-AT-3 (14-30); reverse, 5-ATG-GTG-GGT-TCT-CTG-GTG-3 (64-47); TIMP-2 (36): forward, 5-CAC-CAG-GCC-AAG-TTC-TTC-3 (858- 875); reverse, 5-CGG-TAC-CAC-GCA-CAG-GA-3 (916-900); GAPDH: forward, 5-GAA-GGT-GAA-GGT-CGG-AGT-C-3; reverse, 5-GAA-GAT-GGT-GAT-GGG-ATT-TC-3.

Statistical analysis. The data were expressed as mean ± SD. Statistical analysis was performed using Mann-Whitney's U test and $p<0.05$ was estimated to be significant.

Results

Morphological change of HLE and HLF treated with natural IFN-α and sodium butyrate. As the result of treatment with natural IFN-α and sodium butyrate, the shape and size of HLE and HLF cells were changed. With treatment of IFN-α 1000 U/ml for 7 days, the size of the cells became slightly larger and round-shaped, although hardly changed at 100 U/ml of IFN-α. On the other hand, with treatment of 2 mM sodium butyrate, the size of the cells became larger than that stimulated by IFN-α, especially nuclear size of each cell became larger (Fig. 1). The shape of HLF changed similarly with those of HLE. Apoptosis seemed not to occur in these cells during 7-day culture morphologically and TUNEL assay confirmed that apoptosis was not detected in this culture condition.

Mobility of the HCC cells. The mobility of HCC cells was quantitatively analyzed by digital image analyzer described in Materials and methods. In 2-day culture, HCC cells did not move enough in the observation field for evaluation of the effect of IFN-α and sodium butyrate by this system (data not shown). Therefore, invasion ability of HCC cells should be assayed by other procedures such as the Matrigel assay.

Effect of natural IFN-α and sodium butyrate on the Matrigel invasion activity of human HCC cells. Invasion activity through Matrigel of six human HCC cell lines was examined using Matrigel invasion assay. Invasion activity of HLE and HLF was high but that of other cell lines was very low (HLE, 160±38; HLF, 126±16; HCC-T, 4±2; HCC-M, 13±3; HepG2, 8±7; PLC/PRF/5, 7±6; the number indicated the number of cells invaded into Matrigel, went through small holes, and appeared on the other side of membrane) (Fig. 2). From this result, following experiments were performed using HLE and HLF. These two cell lines were treated with 100 IU/ml and 1000 IU/ml of IFN-α and 2 mM of sodium butyrate for 7 days, and the treated cells were applied on the Matrigel invasion assay. Although 100 IU/ml of IFN-α did not affect invasive ability of two human HCC cells, 1000 IU/ml of IFN-α and 2 mM of sodium butyrate significantly decreased invasive activity of these cell lines [HLE: control vs. IFN-treatment (1000 IU/ml), $p=0.0018$; control vs. SB-treatment, $p=0.0041$; HLF: control vs. IFN-treatment (1000 IU/ml), $p=0.0070$; control vs. SB-treatment, $p=0.0022$; Mann-Whitney's U test] (Fig. 3).

Effect of natural IFN-α and sodium butyrate on MMP-2 and -9 enzymic activities of human HCC cells. Gelatin zymography